

**UNIVERSITÄTSKLINIKUM HAMBURG-EPPENDORF**

Zentrum für Molekulare Neurobiologie Hamburg

Prof. Dr. rer. nat. Matthias Kneussel

**Analysis of Tau phosphorylation in kinesin Kif21b-depleted neurons  
and kinesin-dependent cargo transport under inflammatory  
conditions**

**Dissertation**

zur Erlangung des Grades eines Doktors der Medizin an der Medizinischen  
Fakultät der Universität Hamburg.

vorgelegt von:

Yao Chen  
aus Hunan, China

Hamburg 2024

**(wird von der Medizinischen Fakultät ausgefüllt)**

**Angenommen von der  
Medizinischen Fakultät der Universität Hamburg am: 07.10.2024**

**Veröffentlicht mit Genehmigung der  
Medizinischen Fakultät der Universität Hamburg.**

**Prüfungsausschuss, der/die Vorsitzende: PD Dr. Bastian Cheng**

**Prüfungsausschuss, zweite/r Gutachter/in: Prof. Dr. Matthias Kneussel**

## Table of Contents

1. Introduction .....	1
1.1 Alzheimer's disease .....	1
1.2 Pathogenesis of Alzheimer's disease .....	1
1.2.1 Amyloid $\beta$ and amyloid precursor protein.....	2
1.2.2 Tau and phosphorylation of Tau.....	4
1.3 PI3K/Akt/GSK3 $\beta$ pathway.....	5
1.4 KIF21B .....	6
1.5 Axonal transport.....	7
1.6 KIF21B in neurodegeneration.....	8
1.7 Multiple sclerosis .....	9
1.8 Neuroinflammation .....	11
1.9 Disruption of axonal transport.....	11
2. Aims of the study .....	12
3. Material and methods .....	13
3.1 Animals.....	13
3.2 Isolation of genomic DNA.....	13
3.3 Genotyping .....	13
3.4 Bacteria transformation .....	14
3.5 Midipreps.....	15
3.6 Biochemical experiments.....	15
3.7 Post-nuclear brain lysates and differential centrifugation.....	15
3.8 SDS-PAGE and western blots .....	16
3.9 Primary neuronal culture .....	17
3.10 Immunocytochemical staining.....	17

3.11	Histological experiments .....	18
3.12	Immunohistochemistry.....	18
3.13	Transfection with calcium chloride .....	18
3.14	Treatment and Time-lapse imaging .....	19
3.15	Quantification.....	19
3.16	Statistical analysis .....	19
4.	Results.....	25
4.1	The effect of KiF21B knockout on phosphorylated Tau.....	25
4.2	The impact of KiF21B knockout on phosphorylated Akt .....	26
4.3	The influence of KiF21B knockout on PI3K/Akt/GSK3 $\beta$ signaling pathway ..	27
4.4	The role of KIF21B knockout on phosphorylated Tau at the phenotypic level .....	28
4.5	Axonal trafficking of kinesin-dependent synaptophysin in the initial stages of inflammatory triggers.....	31
4.6	Axonal trafficking of kinesin-dependent BDNF in the initial stages of inflammation.....	35
4.7	Axonal trafficking of kinesin-dependent N-cadherin in the initial stages of inflammatory triggers.....	38
4.8	Axonal trafficking of dynein-dependent LAMP1 in the initial stages of inflammation.....	42
5.	Discussion .....	46
5.1	The role of KIF21B knockout on Tau phosphorylation .....	46
5.2	The effect of inflammatory triggers on bidirectional axonal transport of cargoes .....	47
6.	Conclusion .....	49
7.	List of abbreviations.....	50
8.	References .....	52

9. Abstract.....	59
10. Zusammenfassung .....	60
11. Acknowledgements .....	62
12. Curriculum Vitae .....	63
13. Eidesstattliche Erklärung .....	64

# 1. Introduction

## 1.1 Alzheimer's disease

Alzheimer's disease (AD) is a progressive neurodegenerative disease that features initial memory impairment and cognitive decline that affect behavior, visuospatial orientation, and the motor system, which is the most common form of dementia (Schultz et al., 2004). AD is linked with cognitive decline and it is the leading first cause of death in the world for elderly people (DeTure et al., 2019). Some modifiable risk factors related to dementia include hypertension, less education, hearing impairment, depression, smoking, obesity, physical inactivity, diabetes, and infrequent social contact (Livingston et al., 2020). Some evidence suggests that healthy diets, regular exercise, and improved lifestyle can delay dementia progression and reduce the risk of AD in the elderly population (George et al., 2019). So, early diagnosis and prevention are critical for AD.

AD affects individuals, their families, and the economy. Major clinical features of AD may also include cognitive dysfunction, memory loss, and personality changes (George et al., 2020). Often, selective memory impairment is the first clinical manifestation of AD. The disease is an incurable one; possible treatments for it are only aimed at palliative therapy (Wolk et al., 2016). Therefore, it is crucial to find pathogenesis and therapeutic strategies.

## 1.2 Pathogenesis of Alzheimer's disease

It is well known that the pathological cause of AD is amyloid beta ( $A\beta$ ) plaque in the hippocampus and neurofibrillary tangles (NFTs) consisting of phosphorylated Tau proteins. Even though many hypotheses show that AD pathogenesis touches on Tau hyperphosphorylation, the amyloid cascade, and oxidative stress (Selkoe et al., 1991; Frost et al., 2009). However, hyperphosphorylated Tau and  $A\beta$  cascade are the most proposed theories of pathology.

The cardinal features that appear in progressive Alzheimer's disease due to multiple factors are Tau neurofibrillary tangles and  $A\beta$  plaque formation. All the others include synaptic loss, dysregulation of calcium homeostasis, and finally, all of them—consideration of immune and inflammatory responses. At first, the accumulation of  $A\beta$  in Alzheimer's brain causes postsynaptic hyperexcitability and disturbs synapsis. The

hyperexcitability of neurons leads to increased production of reactive oxygen species and dysregulation of calcium homeostasis (Sehar et al., 2022). A $\beta$  is a vital part of AD pathogenesis.

### **1.2.1 Amyloid $\beta$ and amyloid precursor protein**

Amyloid  $\beta$  is a transmembrane protein by hydrolysis of the amyloid beta precursor protein (APP) through the amyloidogenic pathway. APP is cleaved to C-terminal fragment of Amyloid  $\beta$  (CTF- $\beta$ ) by  $\beta$ -secretase and then different lengths of A $\beta$  peptides by  $\gamma$ -secretase in the amyloidogenic pathway. A $\beta$  peptides include A $\beta$ 42, which is more prone to aggregation and plaque formation than A $\beta$ 40 and has more powerful neurotoxicity (Scheuner et al., 1996; Di Carlo et al., 2012). The accumulation of insoluble A $\beta$  in AD is due to an imbalance between the clearance of these peptides and the production in specific brain parts caused by the inefficient clearance of A $\beta$  peptides.

A $\beta$  toxicity includes excitotoxicity, synaptic dysfunction, altered calcium homeostasis, mitochondrial damage, membrane permeability, oxidative stress, and inflammation (Carrillo-Mora et al., 2014). Finally, this includes the activation of microglia and astrocytes, which evoke associated oxidation and inflammatory responses and ultimately lead to apoptosis and neuronal dysfunction as key processes in the occurrence of AD (Figure 1) (Ujala et al., 2022).

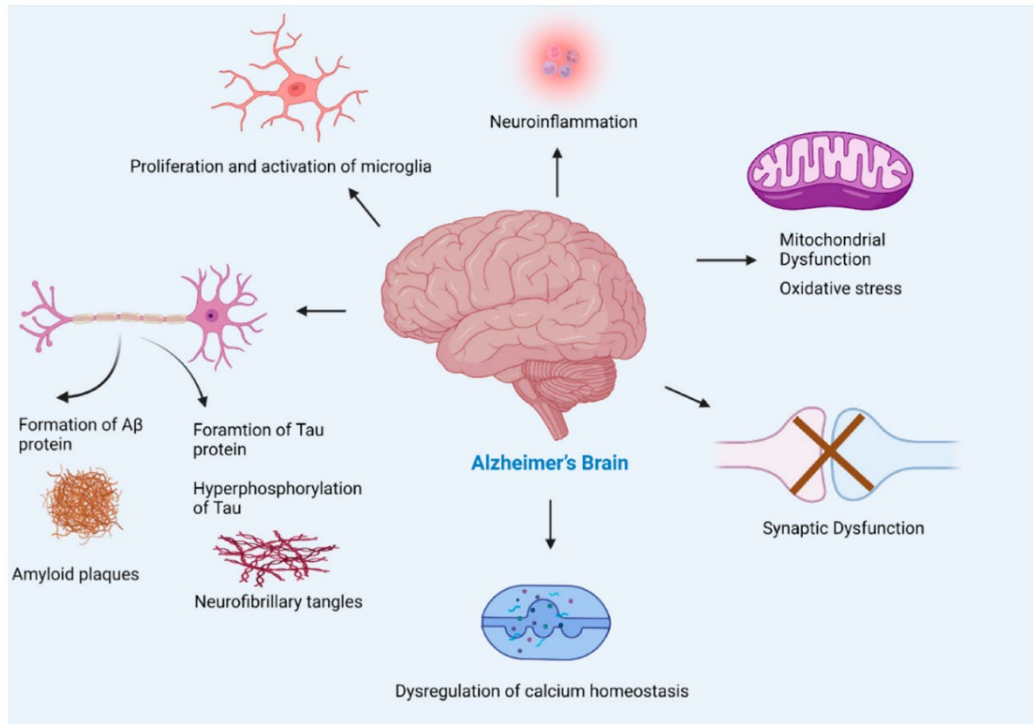


**Figure 1. The pathogenesis of AD.** The cascade of events contributing to AD progression encompasses the formation of A $\beta$  plaques and tau neurofibrillary tangles, culminating in neuronal demise. Concurrently, the activation of microglia, notably clustered around amyloid plaques, precipitates neuroinflammatory responses. This inflammatory milieu, coupled with mitochondrial dysfunction, prompts synaptic loss and perturbed calcium homeostasis. Notably, the accumulation of A $\beta$  disrupts synaptic integrity, instigating postsynaptic hyperexcitability, thereby exacerbating calcium dysregulation and reactive oxygen species production (Ujala et al., 2022).

As pathological effects of A $\beta$  are a significant cause of cognitive decline and AD, in contrast, APP promotes neurite growth in the nervous system. It also involves long-term delay and strengthens synapses by modulating calcium release to increase signaling (Masliah et al., 1992; Kim et al., 2000). Soluble A $\beta$  fragments play many physiological roles, such as long-term potentiation, synaptic plasticity, and neurogenesis. However, it is still being cleared from the brain, as this A $\beta$  binds and oligomerizes others, and then aggregates to form insoluble A $\beta$  plaques. On the other hand, the activation of Tau protein kinase 1 (TPK1) by A $\beta$  leads to the hyperphosphorylation of Tau and promotes the pair helical filaments (PHFs) formation and NFT. The formation of the paired helical filament then continues with the abnormally abundant isoform; then, neurofibrillary tangles can accelerate (Vergara et al., 2019).



## 1.2.2 Tau and phosphorylation of Tau

Tau is a microtubule-associated protein (MAP) (Neve et al., 1986). The most well-established function of Tau proteins is to stabilize axonal microtubules. Tau is found primarily in neuronal axons of the brain that bind to microtubules (MTs) (Regan et al., 2017). Other functions include maintaining axonal transport, signal transmission between neurons, and neuronal structural integrity (Wang et al., 2016). Tau is also a phosphoprotein. The phosphorylation and dephosphorylation of Tau are balanced by protein phosphatase activities that might be regulated by brain development. The development of Tau pathology is a complex multifactorial process. Under normal conditions, Tau has few phosphorylation sites, negatively regulating how Tau binds to microtubules. At the same time, Tau phosphorylation is saturated under pathological conditions (Iqbal et al., 2016).

Tau is hyperphosphorylated and aggregates more readily in the phosphorylated state than in the unphosphorylated state in AD. NFTs are the most characteristic pathological manifestation of AD. It is widely believed that Tau proteins change from a physiological state to a pathological state upon aberrant phosphorylation and then aggregates to PHFs, forming NFTs (Figure 2) (Grundke-Iqbal et al., 1986; Khan et al., 2016). NFTs were considered the neurotoxic form of Tau (Mocanu et al., 2008). However, recent evidence suggests that toxicity may be diffused by soluble low molecular-weight oligomers recognized as NFT precursors (Lasagna-Reeves et al., 2012). Due to its complexity, pathological Tau's pathogenesis remains unclear.

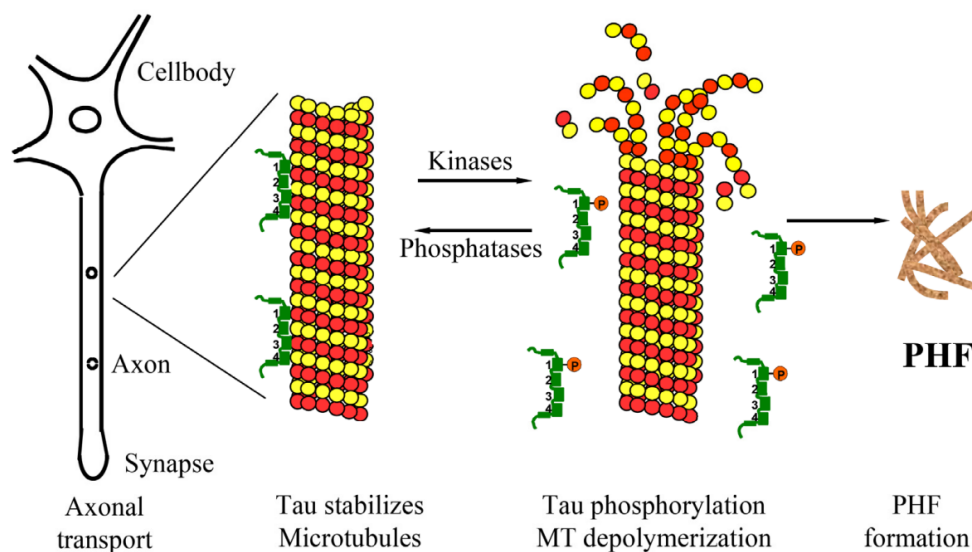


**Figure 2. Tau hypothesis of AD.** Hyperphosphorylation of Tau from dysregulated kinase and phosphatase activity precipitates its dissociation from microtubules. This disrupts the essential role of Tau in stabilizing microtubules, consequently impairing axonal transport. The accumulation of hyperphosphorylated Tau promotes its aggregation into PHF (Mandelkow and Mandelkow, 1998).

Although a primary insult in AD may be increased A $\beta$ , it may ultimately lead to neurodegeneration and cognitive dysfunction by inducing alterations in Tau (Iqbal and Grundke-Iqbal, 2008; Lewis et al., 2001). Loss of function and resulting microtubule instability due to Tau detachment from microtubules, as well as gain of function due to physical interference with intracellular transport by aggregated Tau (Alonso et al., 1996; Dawson et al., 2010; Wolfe et al., 2012). It is unclear how Tau contributes to cognitive decline and neurodegeneration. However, among the most feasible hypotheses for Tau-induced neurotoxicity is to decrease trophic support for neurons (Fahnestock et al., 2011).

### 1.3 PI3K/Akt/GSK3 $\beta$ pathway

The PI3K/Akt cascade can be activated, controlling the activity of several proteins for the survival of neurons, among them Glycogen Synthase Kinase 3 $\beta$  (GSK3 $\beta$ ) (Brunet et al., 2001). GSK3 $\beta$ , as a kinase, phosphorylates threonine and serine sites of various substrates (Hu et al., 2009). GSK3 $\beta$  function is mediated by phosphorylation and de-phosphorylation of different sites. For example, auto-phosphorylation on tyrosine-279/216 regulates GSK3 $\beta$  activation, while phosphorylation on serine sites 21/9 by AKT, protein kinase A and B (PKA-PKB) in the N-terminal leading to its inhibition (Figure 3) (Ly et al., 2013). Most early studies on Tau hyper-phosphorylation explored the kinase-phosphatase imbalance in the brain, identifying GSK3 $\beta$  as a major tau kinase. GSK3 $\beta$  may be involved in developing AD of Tau pathology (Phiel et al., 2003). Many amino-acid residues of the Tau are subject to GSK3 $\beta$  phosphorylation (Chen et al., 2012). It is known that protein-protein interactions take place in binding domains, so GSK3 $\beta$  activated Tau phosphorylation is prone to self-aggregation in a toxic manner (Hernández et al., 2010). GSK3 $\beta$ -mediated phosphorylation of Tau protein occurs near microtubule-binding domains and their amino acid residues (Jackson et al., 2002).

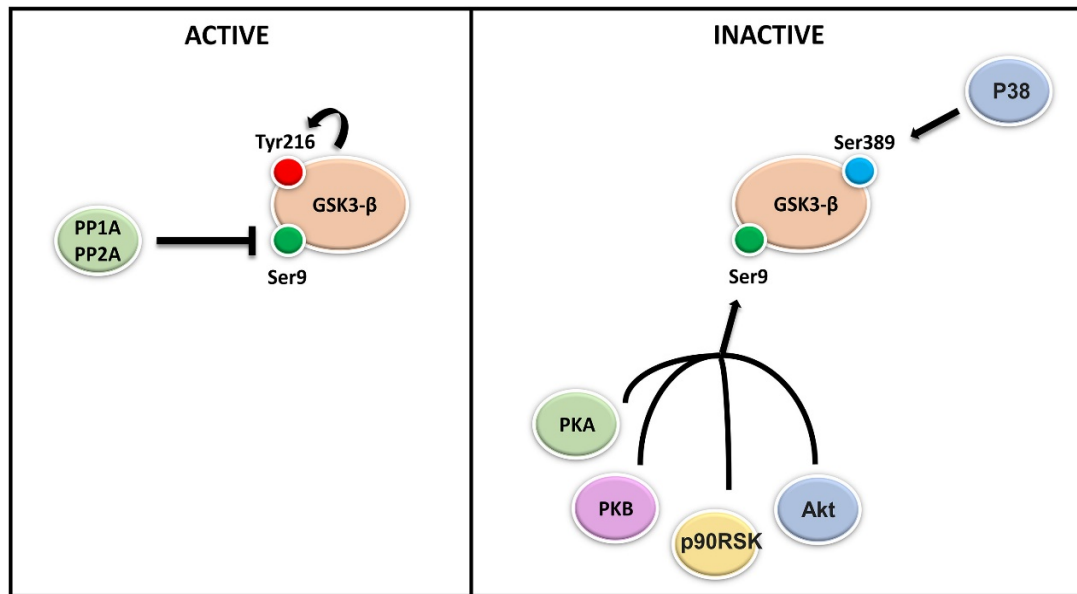


**Figure 3. Regulation of GSK3 $\beta$  activity.** GSK3 $\beta$  exhibits dual activation states, either active or inactive, contingent upon its phosphorylation status. Two enzyme families orchestrate the modulation of GSK3 $\beta$  activity: Serine/Threonine and Tyrosine kinases append phosphate groups to GSK3 $\beta$  and phosphatases, which catalyze the removal of phosphate groups from GSK3 $\beta$  protein in response to extrinsic cues. Experimental findings have elucidated that GSK3 $\beta$  activation entails auto-phosphorylation on tyrosine-216 *in vitro* and *in vivo*. At the same time, its inhibition ensues through phosphorylation on serine nine by a myriad of kinases, including P90RSK, AKT, and protein kinases A and B (PKA-PKB) (Lauretti et al., 2020).

Notably, a hypothesis can be posited that the PI3K/Akt signaling pathway can be activated, thereby inhibiting the phosphorylation activation of GSK3 $\beta$  and subsequent Tau phosphorylation. This hypothesis merits further investigation to elucidate its potential role in tau pathology in AD.

## 1.4 KIF21B

Kinesin superfamily proteins (KIFs) are microtubule-dependent molecular motors and fundamentally affect cellular functions by transporting organelles, macromolecules, and specific proteins (Hirokawa et al., 2015). Kinesin-4 family members (KIF21A and KIF21B) are previously described as sharing little identity with other KIFs beyond the conserved motor domain, suggesting they may play unique roles *in vivo* (Marszalek et al., 1999). KIF21B is present in axons and dendrites, with particular enrichment in the growth cones of developing neurons (Huang and Banker, 2012; Marszalek et al., 1999). It has been confirmed that KIF21B, a classic kinesin protein, could regulate microtubule dynamics (Muhia et al., 2016). On the other hand, KIF21B could inhibit the growth of

microtubules through its tail domain, which acts as a potential microtubule-pausing factor (Labonté et al., 2014).

KIF21B is a key molecular regulator of activity-dependent changes in dendritic trafficking and microtubule dynamics. KIF21B is unique and unmatched in navigating the complex cytoskeletal environment of dendrites, and it is managed by changes in neuronal activity (Ghiretti et al., 2016). Intriguingly, while the typical kinesin motor structural domain determines motor activity, KIF21B-dependent microtubule dynamics regulation is an independent function regulated through the ATP-dependent activity of the C-terminal structural domain of the protein. The neuronal activity must enhance the motility of KIF21B at the expense of microtubule dynamics regulation, the first example of a neuronal kinesin directly regulated by the activity state of the neuron. KIF21B-knockout mice display deficits in learning and memory, consistent with these roles in cargo transport and MT organization (Muhia et al., 2016).

KIF21B may target the PI3K/Akt pathway, and low KIF21B expression might indirectly increase apoptosis and inhibit the proliferation of osteosarcoma cells through the PI3K/Akt pathway (Ni et al., 2021). In conclusion, KIF21B might activate the PI3K/Akt pathway to exert its influence.

## **1.5 Axonal transport**

The most unique morphological features of neurons compared to other cell types are long axons and their extreme polarity (Millecamps et al., 2013). Due to the extreme polarization in the neuron, proper regulation of axonal transport is fundamental for their normal physiological functions. The axonal transport system contains cargoes, motor proteins, microtubules, and adaptors. Motor proteins include dynein and kinesin, which move the cargo along the microtubules (Maday et al., 2014).

Microtubules extend along the axon and function as the cytoskeletal tracks in this transporting process. Kinesins regulate cargo transport along microtubules from the cell body to the terminal within the axon (Hirokawa et al., 2009).

Axonal transport is a highly regulated process and may be modified by posttranslational modification of microtubules, adaptors, phosphorylation of motor proteins and their regulators, and organelle-specific interactions (Wloga et al., 2017). Both kinesins and dynein are activated by baseline autoinhibitory responses and are necessary for the

translocation of each motor along microtubules. In the transport of the kinesin, the Kinesin Heavy Chain (KHC) tail undergoes folding to occlude the KHC motor binding to microtubules, a process resulting in autoinhibition (Mishima et al., 2012). On the contrary, dynein is autoinhibited through dimerization of its motor domains, forming a phi-particle structure. Non-dimerized dynein will be in an open form with higher affinity to the binding site on the microtubule. At the same time, binding with cargo adaptors and dynactin is required to activate motor activity. It is likely to allow processive movement along microtubules by modifying the orientation of motor domains (Zhang et al., 2017).

KIF21B, as a kinesin, regulates dendritic anterograde transport (Muhia et al., 2016). Conversely, microtubule dynamics affect the retrograde biased motility of KIF21B motor teams in neuronal dendrites (Masucci et al., 2022), but its role in axonal transport is not investigated.

## **1.6 KIF21B in neurodegeneration**

KIF21B is expressed in different tissues, with notable enrichment in neuronal dendrites (Marszalek et al., 1999). Elevated levels of KIF21B expression have been associated with the accelerated progression of neurodegenerative diseases (Kreft et al., 2014). Genetic variations within the KIF21B gene are linked to multiple sclerosis (MS) and other inflammatory disorders (Goris et al., 2010; Yang et al., 2015).

In the context of physiological aging among non-demented controls (NDC), no significant alterations were observed in KIF21B expression with advancing age. However, a substantial decline in KIF21B expression was noted with age in MS and AD patients (Figure 4). Moreover, the KIF21B expression of the cortex in AD patients was much higher than the genotype MS risk in NDC and MS patients, and it turned out that those in MS and AD presented a worse condition expressed the KIF21B gene at a significantly higher level. Increased expression was also associated with a shorter time of disease in MS and AD patients, while in MS patients, it was associated with shortened disease duration time and accelerated progression to persistent neurological disability (EDSS 6.0) (Kreft et al., 2014).

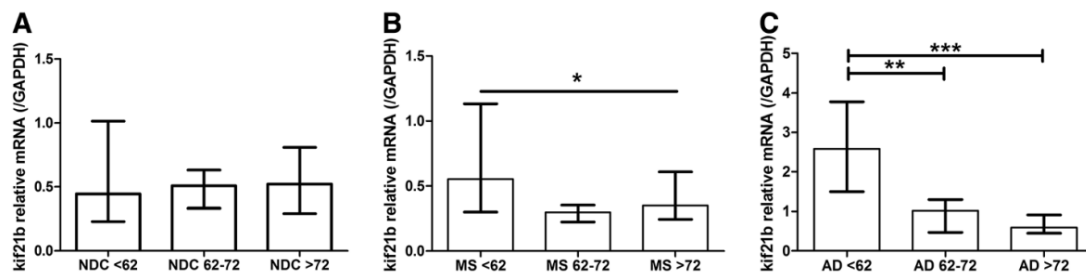


**Figure 4. KIF21B expression in the grey matter.** Expression levels of KIF21B in the grey matter exhibit no discernible changes during physiological aging. However, a notable upregulation of KIF21B expression is evident in young AD patients. KIF21B expression was stratified based on age at death into three distinct categories: individuals in the non-demented control (NDC) group were categorized as <25th percentile (<62 years), those falling between the 25th and 75th percentile were aged between 62 and 72 years, and individuals above the 75th percentile were >72 years old. Comparative analysis of Kif21b expression among these three age categories was performed for (A) NDC, (B) MS, and (C) AD groups (Kreft et al., 2014).

These findings underline the potential role of KIF21B in disease progression in AD and MS. Therefore, investigating KIF21B's involvement in AD and MS pathogenesis is warranted.

## 1.7 Multiple sclerosis

Multiple sclerosis is a prominent inflammatory and degenerative demyelinating disorder of the central nervous system, typically manifesting in early adulthood. Among young and middle-aged individuals, MS represents a primary cause of non-traumatic disability (Dobson et al., 2019). The pathogenesis of MS combines autoreactive T and B cells that are myelin-specific effectors, along with the complement system, pro-inflammatory cytokines, macrophages, astrocytes, and microglia (Nicol et al., 2015; Martin et al., 2016). CD4 T cells, as centers, undergo priming in the periphery against myelin-specific antigens before infiltrating the CNS. CD4 T cells initiate an inflammatory cascade against myelin and oligodendrocytes (OLG), eventually resulting in axonal loss, demyelination, and neurodegeneration in chronic progressive phases (Engelhardt et al., 2022).

Multiple sclerosis is a human neuroinflammatory disease that mirrors experimental autoimmune encephalomyelitis (EAE) in animals, which is driven primarily by CD4 T cells and, to a lesser extent, by CD8 T cells. EAE is induced through active immunization with encephalitogenic antigens emulsified in complete Freund's adjuvant

(CFA) (Figure 5) (Robinson et al., 2014; Karpus et al., 2020). Notably, prior investigations have delineated the reparative aspects of the inflammatory response in neurological disorders, including MS. Immune cells in these conditions exhibit neuroprotective properties by producing neurotrophic factors and interacting with neurons and glial cells to shield them from harm, thereby fostering growth and repair. This phenomenon has been coined "protective autoimmunity" (Graber et al., 2009).

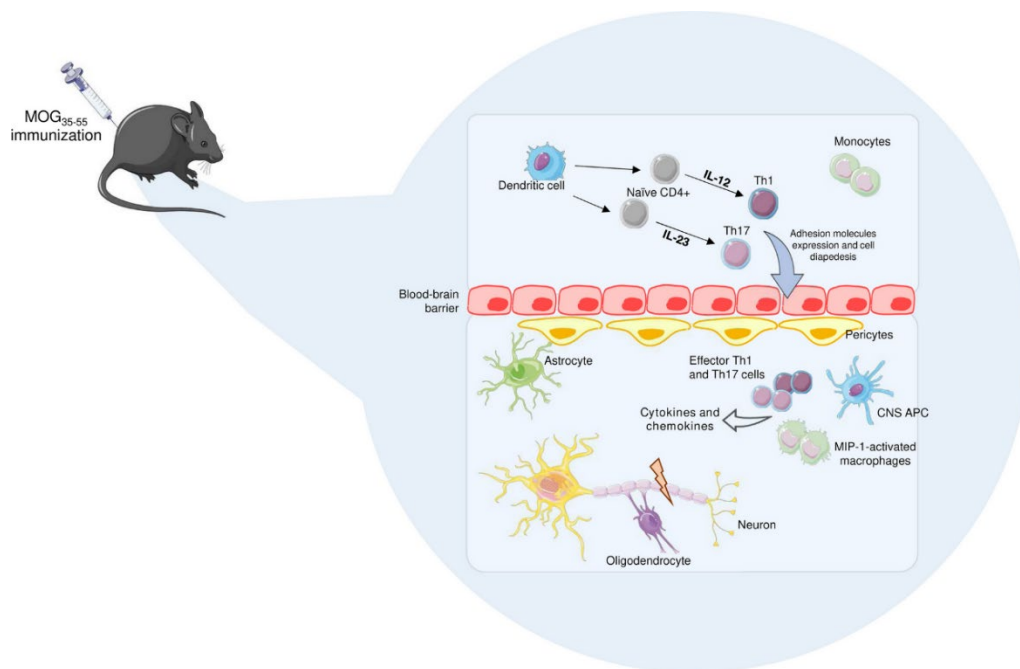


**Figure 5. EAE pathogenesis.** Mice are then actively immunized with the encephalitogenic peptide antigen to induce EAE, used in this experiment: MOG35–55. DCs initiating priming and differentiation of naive T-lymphocytes, which upon activation and further stimulation with IL-23 and IL-12, respectively, differentiate into the Th1 and Th17 phenotypes. On this note, MIP-1 can, through activation, induce the recruitment of monocytes and stimulate the differentiation of those monocytes into macrophages. Those activated cells express adhesion molecules that provide the way for them to cross the BBB endothelium and to penetrate the CNS. APCs within the CNS further bolster myelin-specific Th17 and Th1 effector responses and macrophage activation. The ensuing activation of these cells culminates in the production of chemokines and pro-inflammatory CKs, contributing to myelin damage. (<https://creativecommons.org/licenses/by/3.0/>).

Abbreviations: Myelin oligodendrocyte glycoprotein 35–55 (MOG35–55); Peripheral dendritic cells (DCs); T helper 1 (Th1); Interleukin-12 (IL-12); Macrophage inflammatory protein-1 (MIP-1); Blood brain barrier (BBB); Antigen-presenting cells (APCs); Cytokines (CKs)

## **1.8 Neuroinflammation**

Impaired axonal transport, a hallmark feature of many neurodegenerative diseases, can exacerbate axon degeneration. In neuronal inflammation, which accompanies several neurodegenerative disorders such as MS, defects in MT bundling occur within axons, precipitating axonal degeneration (Hahn et al., 2019). Inflammatory stimuli can induce microtubule composition and dynamics changes through various signaling pathways (Dubey et al., 2015). MS, a prevalent neuroinflammatory condition, manifests progressive axon degeneration, yet the timing and mechanisms underlying alterations in axonal transport in this context remain elusive. Extensive deficits in transport machinery and diminished delivery of distal organelles, notably mitochondria, might contribute to axonal dystrophy during advanced stages of the disease (Sorbara et al., 2014). However, the precise identity of the motor proteins affected at the onset of inflammation remains poorly characterized.

## **1.9 Disruption of axonal transport**

These diseases occur with rather different phenotypic expressions at the clinical level, sharing, however, a selective vulnerability of subgroups of polarized neurons with their long axons. Axonal degeneration and synaptic retractions are prominent early events across various neurodegenerative diseases, preceding cell death (Hirano et al., 1984; Stokin et al., 2005; Gilley et al., 2012). A fundamental inquiry into the role of axonal transport in neurodegeneration pertains to whether disruption of axonal transport is merely a consequence or a pivotal instigator of the disease process. Notably, the function of axonal transport is indispensable for maintaining neuronal health. The significance of meticulously regulated axonal transport in neuronal health is underscored by the observation that mutations in motor proteins are closely linked to neurodegenerative pathologies.



## **2. Aims of the study**

Previous research has established KIF21B as a kinesin superfamily member, with upregulated expression levels linked to the accelerated progression of AD and MS. However, the mechanism of KIF21B in AD and MS remains unclear. Therefore, the role of KIF21B in Tau phosphorylation needs to be explored. At the same time, its impact on neuroinflammation in MS is also part of the doctoral investigation. A constitutive knockout KIF21B mouse strain (KIF21B KO) was employed and thoroughly characterized to accomplish these objectives. The primary goals include analyzing the influence of KIF21B knockout in Tau phosphorylation and axonal transport of kinesin-dependent or dynein-dependent cargoes under inflammatory conditions.

### 3. Material and methods

#### 3.1 Animals

In this scientific inquiry, Kif21b knockout (-/-) mice were created through the utilization of knockout first embryonic stem (ES) cells sourced from the Knockout Mouse Project repository (KOMP, clone No. 24702). The employed targeting strategy successfully permanently eliminated Kif21b gene expression in the -/- mice (Muhia et al., 2016). Subsequently, Kif21 -/- mice were accommodated and propagated within the University Medical Center Hamburg-Eppendorf animal facility.

#### 3.2 Isolation of genomic DNA

Genomic DNA was extracted from tail biopsies or ear punches of 3- to 4-week-old mice to obtain the experimental mouse genotypes. For DNA extraction, incubate for 15 min at 65°C using a Rapid Extraction Buffer (Biozym Scientific GmbH, Hessisch Oldendorf, Germany). It was then heat-inactivated for 2 minutes at 95°C.

#### 3.3 Genotyping

Genotyping and PCR confirmation Genomic DNA was extracted from tail biopsies using Quickextract (Biozym, Hessisch Oldendorf) and processed for PCR using the following primers (Table 1). The following reaction mixture (Table 2) was used to amplify the KIF21B exon using a template and primers, and the genomic DNA was isolated from tail biopsies. PCR was carried out by using a PTC-200 thermocycler (MJ Research) and a genotyping PCR program (Table 3). The presence of the wild type and knockout alleles was indicated by 727 and 15617 bp products, respectively, which were detected on a 1.5% agarose gel.

**Table 1- Genotyping PCR primers**

Primers	Sequence
WT sense	5'-CCCTGGTGTTCCCTTTCTTCTC-3'
WT and KO antisense	5'-AAACCTGGGCAAAGGCATAC-3'
KO sense	5'-GAAATGACCGACCAAGCGACG-3'

**Table 2-Genotyping PCR reaction master mix**

Stocks	Reaction mix(25µl)
Buffer 10×	2.5 µL
dNTPs(2.5mM)	0.5 µL
Primer Forward (PrFw)(10mM)	0.5 µL
Primer Reverse A (PrRVA)(10mM)	0.25µL
Primer Reverse B (PrRVB)(10mM)	0.25µL
Template DNA	0.5 µL
Taq Polymerase(5U/l)	0.15 µL
ddH <sub>2</sub> O	20.35 µL

**Table 3-Genotyping PCR program**

Step	Temperature	Time	Function
a	98°C	2 minute	Initial denaturation
b	98°C	30 seconds	Denaturation
c	66°C	45 seconds	Annealing
d	72°C	30 seconds	Extension
e	Go to step b x 35 times	-	Cycling reaction
f	72°C	10 minutes	Final extension
g	4°C	Pause	Hold

### 3.4 Bacteria transformation

DH5α fertile E. coli cells were transformed using a heat shock protocol. 100uL of the bacterial cells were incubated with the DNA on ice for 30 minutes. The mixture was incubated in a water bath at 42 °C for 45 seconds and then placed on ice for 45 seconds to induce heat shock. Bacterial recovery was accomplished by adding S.O.C. medium at 37 °C incubation conditions. Recovery incubation time was based on the antibiotic resistance of the plasmid: 45 min for Kanamycin and 30 min for Ampicillin.

### **3.5 Midipreps**

LB bacteria are cultured overnight in 100 mL of LB medium supplemented with antibiotics. They were then centrifuged at +4°C for 10 min at 5000 rcf. After the extraction, DNA was purified using the Nucleobond Xtra Midi EF DNA extraction kit following the manufacturer's instructions. To elute DNA, add 3.5 mL of isopropanol and mix the two phases. The samples were centrifuged at 15,000g for 30 min at +4°C in an Avanti J-26 XP, using a fixed angle JA-25.50 spinning rotor. The resulting pellet was quickly washed in 70% EtOH and air-dried further under room temperature for 30 min. Resuspend the DNA pellets in endotoxin-free water and take the concentration and purity of DNA using spectrophotometric techniques.

### **3.6 Biochemical experiments**

All biochemical experiments were performed in protease and phosphatase inhibitors in an ice-cold solution, which were standard conditions. All the centrifugations were performed at +4°C and all the mice were sacrificed by carbon dioxide (CO<sub>2</sub>) and guillotine. Embryonic brain dissection was carried out in ice-cold glucose-supplied PBS.

### **3.7 Post-nuclear brain lysates and differential centrifugation**

The total brains were put into a buffer containing an ice-cold IM-Ac buffer. The organization was homogenized eight times at 900 revolutions per minute. Post-nuclear lysate (S1) was the supernatant obtained by centrifuging the homogenate at 1000 xg for 10 min at +4°C and preserved. The protein concentration was determined with the Pierce™ BCA Protein Assay Kit. Accordingly, the samples were diluted with buffer IM-Ac to make the sample volume even.

A differential centrifugation methodology was employed to segregate distinct subcellular fractions from the post-nuclear lysate (S1). Specifically, the post-nuclear S1 fraction was treated with 1% Triton X-100. It is then lysed on a rotating wheel for 30 min. The resultant post-nuclear S1 fraction was then subjected to centrifugation at 10,000 xg for 10 minutes, yielding the S2 supernatant. All centrifugation steps were executed at +4°C to maintain sample integrity. Finally, 4x SDS loading buffer was introduced, and the samples were heated at 95°C for 5 min.

### 3.8 SDS-PAGE and western blots

In SDS-PAGE protein, the different cast gel concentrations are as follows: after the separating gel had polymerized, 5% of acrylamide stacking gel was added to the top of it in a sandwich with polyacrylamide gel. After polymerization, samples were loaded into the back-up chamber with 1x SDS running buffer preloaded in. We loaded 5  $\mu$ L of protein ladder marker and sample onto the stacking gel of the prepared gel. Subsequently, the proteins separated in the SDS-gel are blotted wet or semi-dry onto the PVDF membrane. Pre-activation of the PDVF is done in both cases using 100% MeOH. After blotting, 5% milk/TBST blocking membrane was used for standard experiments.

For WB involving phosphorylated antigens, 5% IgG-free BSA was used as the blocking solution. The primary and secondary antibodies were then diluted with the same solution as in the blocking step. After blocking, the membrane was incubated overnight at +4°C with the primary antibody, depending on the antibody. The membrane is then rinsed with TBST three times for 5 minutes each time and incubated with horseradish peroxidase (HRP)-conjugated secondary antibody or IRDye® secondary antibody for 1 hour at room temperature. The membrane was then washed thrice with 15 mL volumes of TBST each time for 5 min. The membrane was then developed with the ECL containing HRP substrate solution, and finally, the images were developed in an imager of Intas ECL Chemostar. Besides, images were taken by an Odyssey CLx (LI-COR) imaging device. Stripping was allowed at room temperature and then probed for other proteins using the same membrane within 30 min. The membrane was incubated with TBST, re-blocked, and re-probed at room temperature according to the above protocol. The signal intensity of the bands was determined using Image Studio Lite (version 5.2, LI-COR) or Fiji (ImageJ, version 2.0, NIH, USA).

Primary antibodies were AT270 (MN1050, Thermo Fisher), Tau (A0024, Dako), Phospho Akt (4060, Cell Signaling), Akt (2920, Cell Signaling), Anti-GSK3 (alpha + beta) (phospho Y216 + Y279) ( ab45383, Abcam), Anti-GSK3 beta + GSK3 alpha (ab185141, Abcam) and  $\gamma$ -adapatin(610386, BD Transduction Lab).

### **3.9 Primary neuronal culture**

Pregnant females were used in this study, and all the animals were humanely killed by CO<sub>2</sub> asphyxiation and later by cervical dislocation. The brains of the embryos were removed using scissors after decapitating them. The isolated brains were from primary neuronal cultures of either the embryos' cerebral cortex or hippocampus, which were between embryonic days 15 and 17 of age. After decapitation, the brains were removed and dissected in an ice-cold, autoclaved glucose/PBS buffer to remove meninges and isolate the hippocampus and cortical regions. When the embryo's genotype was undetermined, a cerebellar biopsy was obtained for subsequent PCR genotyping, while the corresponding hippocampi and cortexes were preserved in the Hibernating medium. Dissociation of the cells was done using incubation in 0.05% EDTA-Trypsin solution for 5 min at 37°C. The reaction of trypsin with the dissociated tissue was terminated by washing with prewarmed HBSS containing 10% FBS. Tissues were then transferred into pre-warmed HBSS and with two fire-polished glass pipettes, trituration was affected mechanically through suction. The dissociated cells were seeded into various recipient plates based on their intended experimental use: immunofluorescence stained coverslips were grown in 24-well plates, and the same type of cells was used for time-lapse imaging experiments, grown on 6-well plates seeded with autoclaved 25 mm glass coverslips. Before cell seeding, all coverslips were coated overnight with a 1:200 poly-L-lysine solution in PBS, followed by two washes with sterile ddH<sub>2</sub>O. Pre-warmed Lonza Primary Neuronal Growth Medium (PNGM) supplemented with 1% penicillin-streptomycin and 1% L-Glutamine was then added to the coverslip in preparation for cell seeding.

### **3.10 Immunocytochemical staining**

Briefly, DIV14 hippocampal neuronal cultures were rinsed with PBS and fixed in 4% PFA solution prepared in PBS with 4% sucrose. After that, cells were twice washed with PBS and permeabilized with PBS/1%BSA + 0.1% Triton-X. Primary antibodies (List of antibodies) were diluted in PBS/ 1%BSA and incubated overnight at 4°C. These cells were then incubated with fluorochrome-conjugated secondary antibodies and fluorochrome conjugated (e.g., DAPI) in PBS/1%BSA for 1 h at room temperature, washed for three times in PBS, and then counterstained with DAPI (1 µg / mL) for 30 min at room temperature. The nuclei of the cells were fluorescence-stained. Finally,

after that, another three washes were done with PBS before mounting using Aqua Poly Mount. Images were taken on a Zeiss LSM 900 confocal microscope.

### **3.11 Histological experiments**

Following the euthanasia of the animals via CO<sub>2</sub> inhalation and subsequent cardiac perfusion with 4% PFA/PBS, mice aged between 41-42 weeks were subjected to anesthesia. The next day, the brains were carefully extracted and post-fixed upon perfusion for 12 hours in 4% PFA/PBS. Then, the dehydration step was performed over a 48-hour period in 30% sucrose/PBS. Brain samples were then snap-frozen in dry ice and embedded in TissueTek (catalog number 4583, Sakura Finetek) and stored at -80°C. Coronal sections of the cerebral cortex, measuring 18µm in thickness, were obtained using a tissue slicer. These sections were then preserved in an antifreeze solution at -20 °C until further analysis.

### **3.12 Immunohistochemistry**

The coronal sections were allowed to thaw and were washed in PBS. Permeabilization was done in all cases using Triton X-100/TBST for 20 minutes. The sections were blocked in 10% NGS/ TBST for 1 hour at room temperature after the three washes with TBST. The primary antibodies were incubated overnight at 4°C in a wet chamber. The next day, after three washes with TBST, the secondary antibodies were incubated for one hour at room temperature in a wet chamber before rewashing. Finally, washed 3 times in the last step with Aqua Poly Mount. The primary antibodies used were: AT8 (MN1020, Thermo Fisher) and Tau (A0024, Dako). Neurons were counterstained with DAPI 1:1000 along with secondary antibodies. Image acquisition was conducted using a Zeiss LSM 900 confocal microscope. Subsequent image processing was performed utilizing Fiji (ImageJ, version 2.0), followed by quantitative analysis using MetaMorph software.

### **3.13 Transfection with calcium chloride**

Primary neuronal cultures were transfected using the calcium chloride (CaCl<sub>2</sub>) method. The transfection of cell lines is performed at 60% confluency of the cells. Briefly, the cocktail included approximately 0.75 µg DNA, 1M CaCl<sub>2</sub>, and water for the 25 mm coverslips. The mixture was then added dropwise to 2X HEPES-buffered saline

(2xHBS). The reconstituted mixture was vortexed and incubated at room temperature for 20 min. 90-120 min of incubation with this mix followed the addition of the mix to the cells. For primary neuronal cultures, transfection was started with DIV12. Then rinse twice with HEPES buffer pre-heated to 37°C. The previously saved conditioned medium was re-added into the cells.

### **3.14 Treatment and Time-lapse imaging**

In this study, DIV12 cortical neurons were utilized as the experimental model. These neurons were transfected to express specific cargo proteins, including Synaptophysin-GFP, mCherry-BDNF, N-cadherin-RFP and Lamp1-RFP with volume maker (GFP or Ruby). The experimental conditions involved exposing these transfected neurons to an inflammatory cocktail (IC) comprising IFN- $\gamma$ , TNF- $\alpha$ , and rmlL-17 for a period of 48 hours, with comparisons made to non-treatment controls (Meyer-Arndt., 2023).

Following the designated exposure period, transfection efficiency was assessed using a standard epifluorescence microscope. Further, the cells are transferred into the imaging chamber, Time-lapse Imaging HEPES Buffer. Imaging is done with the spinning disk confocal microscope and a CCD camera along with Visitron system, both with specified conditions of 5% CO<sub>2</sub> and 37°C. Cellular imaging and recording were performed using a 60x oil objective lens.

### **3.15 Quantification**

For Time-lapse Imaging quantification, the focus was on neuronal axons with anterograde and retrograde movement. Quantification was performed using a manual tracking plugin from Fiji (ImageJ, version 2.0) and Kamograph. Absolute speed was considered for statistical analysis.

### **3.16 Statistical analysis**

Each experiment was replicated independently at least three times. Statistical analyses were conducted using Prism software (GraphPad, version 9.0.1). Initially, an exploratory data analysis was performed to detect outliers, followed by assessments of normality using Kolmogorov-Smirnov or Shapiro-Wilk tests. The means of normally distributed data were compared either by the two-tailed unpaired Student t-test or by



two-way analysis of variance (ANOVA), while those of non-parametrically distributed data were compared using the Mann-Whitney test or Kruskal-Wallis test. The graphs were plotted using either Excel (Microsoft, Redmond, WA, USA) or Prism software. Bar diagrams were employed for normally distributed data. Individual data points were displayed as dots when the sample size (n) was less than 10. Data presentation adhered to the convention of mean  $\pm$  standard error of the mean (SEM).

### 3.17 List of solutions

Solution	Chemical composition
10X PBS	1.37M NaCl / 27mM KCl / 18mM KH <sub>2</sub> PO <sub>4</sub> / 100mM Na <sub>2</sub> HPO <sub>4</sub>
2XHBS	280mM NaCl / 10mM KCl / 1.5mM Na <sub>2</sub> HPO <sub>4</sub> / ddH <sub>2</sub> O / 50mM HEPES / 12mM dextrose / pH=7.5 adjusted with 0.5M NaOH
10X TBST	200mM Tris-Base / 1.5M NaCl / 1% Tween
50X TAE	242g Tris-Base / 57.1ml glacial Ac. Acid / 0.5M EDTA pH=8 for 1L
10X SDS Running Buffer	250mM Tris / 15% SDS / 2.5M Glycine / ddH <sub>2</sub> O / pH=8.3 for 1L
4X SDS Loading Buffer	200mM Tris-HCl / 4% BME / 0.016% Bromophenol Blue / 24% Glycerol / 8% SDS
CaCl <sub>2</sub>	1M Calcium Chloride
HEPES Buffer for Time-lapse Imaging	10mM HEPES / 135mM NaCl / 5mM KCl / 2mM MgCl <sub>2</sub> / 2mM CaCl <sub>2</sub> / 15mM Glucose / pH=7.4
IHC Antibody incubation buffer	TBST / 1 % NGS
IHC Blocking Buffer	TBST / 10 % NGS
IHC Perfusion and Fixation Buffer	PBS / 4% PFA
IHC Dehydrating buffer	PBS/30% sucrose
Saline	H <sub>2</sub> O / 0.09% NaCl
Antigen retrieval buffer	10mM Na-citrate / 0.05% Tween/ PH=6.0
PBS / Triton Lysis Buffer	PBS / Triton X-100 1% + prot./phosp. inhibitors
DHPG incubation buffer	145mM NaCl / 2.5mM KCl / 1mM MgCl <sub>2</sub> / CaCl <sub>2</sub> / 10mM HEPES / C <sub>6</sub> H <sub>12</sub> O <sub>6</sub> / pH=7.4 adjusted with 0.5M NaOH
SDS-Transfer Buffer	25mM Tris / 192mM Glycine / 20% MeOH

IM-Ac buffer	20mM HEPES / 40mM KCl / 5mM MgCl <sub>2</sub> / 100mM CH <sub>3</sub> CO <sub>2</sub> K / 5mM EGTA / 1mM PMSF / 5mM DTT + prot./phosp. Inhibitors / pH=7.2 adjusted with 0.5M NaOH.
Blotting Buffer (Wet)	48mM Tris / 39mM Glycin / 0.037%SDS % / 20%MetOH
Blotting Buffer (Semi-dry)	25mM Tris / 150mM Glycin / 20%MetOH
Stripping Buffer	25mM Glycine / 1%SDS / pH=2.0

### 3.18 List reagents

Reagent	Catalog #.	Company
Aqua-Poly/Mount	18606-20	Polysciences
Acrylamide/Bis- acrylamide	A3699	Sigma-Aldrich
(RS)-3,5-DHPG	0342	R&D Systems
Ampicillin sodium salt, 10 g	K029.1	Carl Roth GmbH and Co. KG
Ammonium peroxydisulphate(APS), 1 kg	9592.1	Carl Roth GmbH and Co. KG
Bovine Serum Albumin(BSA)	A3156	Sigma-Aldrich
5-alpha Competent E. coli	C2989K	New England BioLabs
1,4-Dithiothreitol (DTT), 5 g	6908.1	Carl Roth GmbH and Co. KG
Dulbecco's Modified Eagle Medium (DMEM)	61965026	Thermo Fisher Scientific
1 Kb DNA ladder	15615-016	Invitrogen Life Technologies
Deoxynucleotide Triphosphates (dNTPs)	U1240	Promega
Ethanol, 2.5 l	9065.4	Carl Roth GmbH and Co. KG
Paraformaldehyd (PFA), 1 kg	0335.3	Carl Roth GmbH and Co. KG
HBSS Buffer	14170-088	Invitrogen Life Technologies
Glutaraldehyde solution (GA)	G5882	Sigma-Aldrich
Hibernate™-E Medium	A1247601	Thermo Fisher Scientific

Phenylmethylsulfonyl fluoride (PMSF), 5 g	6367.1	Carl Roth GmbH and Co. KG
2-Propanol, 2.5 l	6752.2	Carl Roth GmbH and Co. KG
Kanamycin, 50 g	T832.3	Carl Roth GmbH and Co. KG
PhosSTOP (inhibit table for phosphatase)	04906845001	Sigma-Aldrich
Pierce™ ECL Western Blotting Substrate	32106 / 32109 / 32209	Thermo Fisher Scientific
Sodium dodecyl sulfate(SDS)	L4509	Sigma-Aldrich
PNGM™ Primary Neuron Growth Medium	CC-4461	Lonza Bioscience
Poly-D-Lysin -hydrobromid	P7886	Sigma-Aldrich
cOmplete™, EDTA-freier Proteasehemmer-Cocktail	04693132001	Roche
Protease inhibitors set	11206893001	Roche
TMEDA	T9821	Sigma-Aldrich
Triton® X 100, 1 l	3051.2	Carl Roth GmbH and Co. KG
BlueStar Plus Prestained Protein Marker	MWP04	NIPPON Genetics
PVDF Blocking Reagent for Can Get Signal™	TYB-NYPBR01	Cosmo Bio LTD
Rhodamine Phalloidin	PHDR1	Cytoskeleton, Inc.
Trypsin-EDTA	25300054	Invitrogen Life Technologies
TNF-α	300-01A-50UG	Peprotech
rmIL-17	7956-ML/CF	R&D system
IFN-γ	300-02-100UG	Peprotech

### 3.19 List of primary antibodies

Antibody	Species	Catalog #.	Company	Application
Phospho-Tau(AT270)	Mouse	MN1050	Thermo Fisher Scientific	WB 1:1000

Phospho-Tau (AT8)	Mouse	MN1020	Thermo Fisher Scientific	IHC 1:200
pan Tau	Rabbit	A0024	Dako	WB 1:2000 IHC 1:300
Phospho-Akt	Rabbit	4060	Cell Signaling Technology	WB 1: 1000
pan Akt	Mouse	2920	Cell Signaling Technology	WB 1:1000
GSK3 (alpha + beta) (phospho Y216 + Y279)	Mouse	ab45383	Abcam	WB 1:1000
GSK3 beta + GSK3 alpha	Rabbit	ab185141	Abcam	WB 1:2000
$\gamma$ Adaptin	Mouse	610386	BD Transduction Lab	WB 1:2000

### 3.20 List of secondary antibodies

Antibody	Catalog #.	Company	Application
Alexa Fluor® 488 donkey anti-rabbit IgG (H+L)	711-546-152	Jackson ImmunoResearch	IHC 1:1,000
Cy™3 goat anti-mouse IgG, light chain specific	115-165-174	Jackson ImmunoResearch	IHC 1:1000
Peroxidase-conjugated donkey anti-rabbit IgG (H+L)	711-036-152	Jackson ImmunoResearch	WB 1:15,000
Peroxidase-conjugated donkey anti-mouse IgG, light chain specific	115-035-174	Jackson ImmunoResearch	WB 1:15,000
Peroxidase-conjugated donkey anti-mouse IgG (H+L)	715-036-151	Jackson ImmunoResearch	WB 1:15,000
IRDye®680RD goat anti-mouse IgG	926-68070	LI-COR	1: 10,000
IRDye®800CW goat anti-rabbit IgG	926-32211	LI-COR	1: 10,000

### 3.21 List of Plasmids

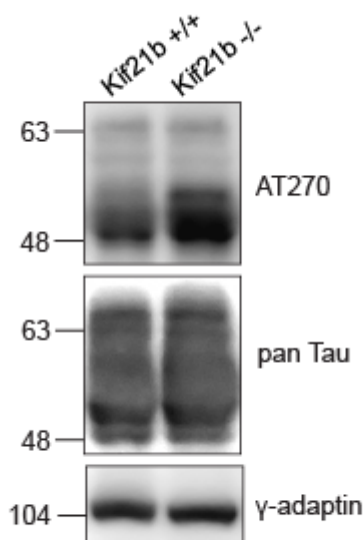
Plasmids	Catalog #.	Provider
Lamp1-RFP	1817	Addgene
Synaptophysin-GFP	137188	Addgene
N-cadherin-RFP	-	Dr. Heisler FF
mCherry-BDNF	191144	Addgene
GFP	65436	Clontech
Ruby	160906	Clontech

## 4. Results

### 4.1 The effect of Kif21B knockout on phosphorylated Tau

Considerable evidence indicates that elevated levels of KIF21B are related to the accelerated progression of AD (Kreft et al., 2005). However, the mechanism of action of KIF21B and AD remains unclear. To clarify whether and how KIF21B knockout affects Tau phosphorylation, western blotting was performed to detect the levels of phosphorylated Tau in the brain-isolated lysate supernatant S2 of KIF21B knockout (Kif21b  $-/-$ ) and wild-type (Kif21b  $+/+$ ) mice. Western blotting bands showed a significant enhancement in AT270 protein bands in Kif21b  $-/-$  brain-isolated lysate compared with Kif21b  $+/+$  brain-isolated lysate (Figure 6A). Quantitative western blot analysis showed a significant increase in phosphorylated Tau (AT270) normalized to pan Tau in brain lysates of Kif21b  $-/-$  mice compared to brain lysates of Kif21b  $+/+$  mice ( $p=0.0141$ ) (Figure 6B). This finding confirms that an accumulation of phosphorylated Tau in the brains of Kif21b  $-/-$  mice and AD might be associated with KIF21B.

**A**



**B**

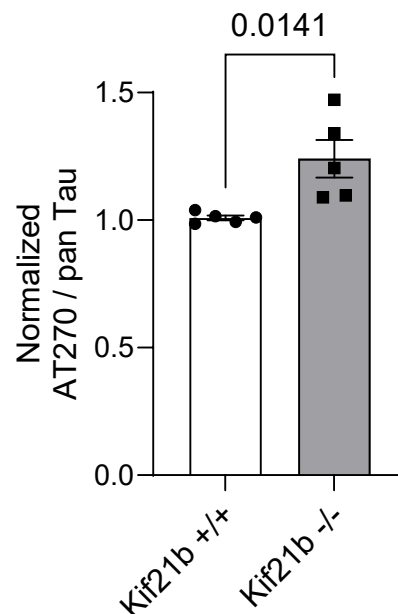


**Figure 6. Phosphorylated Tau is upregulated in Kif21b  $-/-$  mice.**

**A.** Western blot bands of Tau phosphorylation from brain lysates of 41-42 weeks mice, including Kif21b  $+/+$  mice and Kif21b  $-/-$  mice. Phosphorylated Tau was detected using the AT270 antibody, while total Tau was detected using the pan Tau antibody.  $\gamma$ -adapitin was used in the loading control.

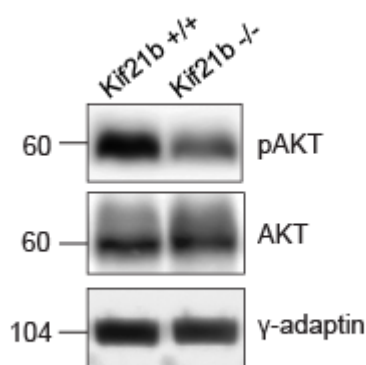
**B.** Quantification of phosphorylated Tau signal intensities, probed with AT270 and normalized to pan Tau as depicted in (A) (n = 5 mice per genotype). P value was determined using a two-sided unpaired Student's t-test. The data are presented as mean  $\pm$  standard error of the mean (SEM).

## 4.2 The impact of KIF21B knockout on phosphorylated Akt

It has been certified that phosphorylated Tau is upregulated in Kif21b  $-/-$  mouse brain lysates. On the other hand, some data report that activation of the PI3K/Akt signaling pathway inhibits GSK3 $\beta$  activation, reducing phosphorylated Tau (Lauretti et al., 2020). The levels of Akt phosphorylation were assessed in brain lysates from Kif21b  $-/-$  and Kif21b  $+/+$  mice to clear further the upstream signaling pathways involved in Tau phosphorylation by KIF21B knockout.

The western blot bands were shown in Figure 7A. Quantification of western blotting showed that the level of phosphorylated Akt normalized to Akt was significantly decreased in brain lysates from Kif21b  $-/-$  mice compared to brain lysates from Kif21b  $+/+$  mice ( $p=0.0079$ ) (Figure 7B). The results suggest that the PI3K/Akt signaling pathway may be involved in KIF21B knockout acting on Tau phosphorylation.

**A**



**B**

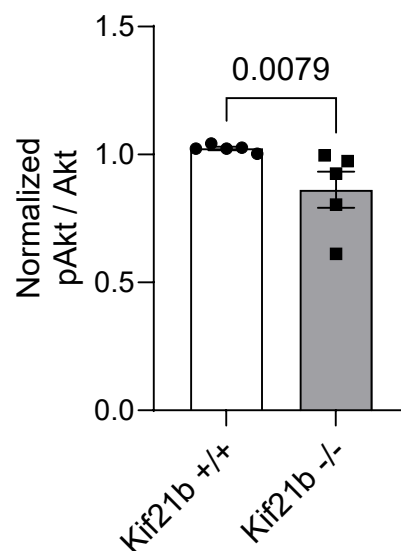


**Figure 7. Phosphorylated Akt is decreased in Kif21b  $-/-$  mice**

**A.** Western blot analysis was conducted to evaluate the level of Akt phosphorylation using brain lysates obtained from mice aged 41 to 42 weeks, encompassing both Kif21b  $+/+$  (wild-type) and Kif21b  $-/-$  (knockout) mice. Phosphorylated Akt (pAkt) and total Akt levels were assessed, with  $\gamma$ -adapatin as the loading control.

**B.** The signal intensities of phosphorylated Akt, probed with pAkt, were quantified and normalized to total Akt levels, as depicted in (A). A total of  $n = 5$  mice per genotype were included in the analysis. Statistical significance was determined using a Mann-Whitney test. The data are presented as mean  $\pm$  SEM.

### 4.3 The influence of KIF21B knockout on PI3K/Akt/GSK3 $\beta$ signaling pathway

The next step was to explore whether, upon reduction of activation of the PI3K/Akt pathway, KIF21B knockout subsequently increases the GSK3 $\beta$  (Tyr216) level, possibly leading to increased phosphorylated Tau levels. Therefore, western blotting was used to detect GSK3 $\beta$  (Tyr216) levels in isolated lysed supernatant S2 from the brains of Kif21b  $-/-$  and Kif21b  $+/+$  mice.

Western blot bands targeted phosphorylated GSK3 $\beta$  (Tyr216) in its activated state (Figure 8A). The results of the study revealed a significant increase ( $p=0.0154$ ) in phosphorylated GSK3 $\beta$  (Tyr216) normalized to total GSK3 $\beta$  in brain lysates from Kif21b  $-/-$  mice compared to brain lysates from Kif21b  $+/+$  mice (Figure 8B).

All of the above results indicate that KIF21B knockout decreased the level of phosphorylated Akt, increased the level of GSK3 $\beta$  (Tyr216), and increased the level of phosphorylated Tau in the brain lysate of mice.

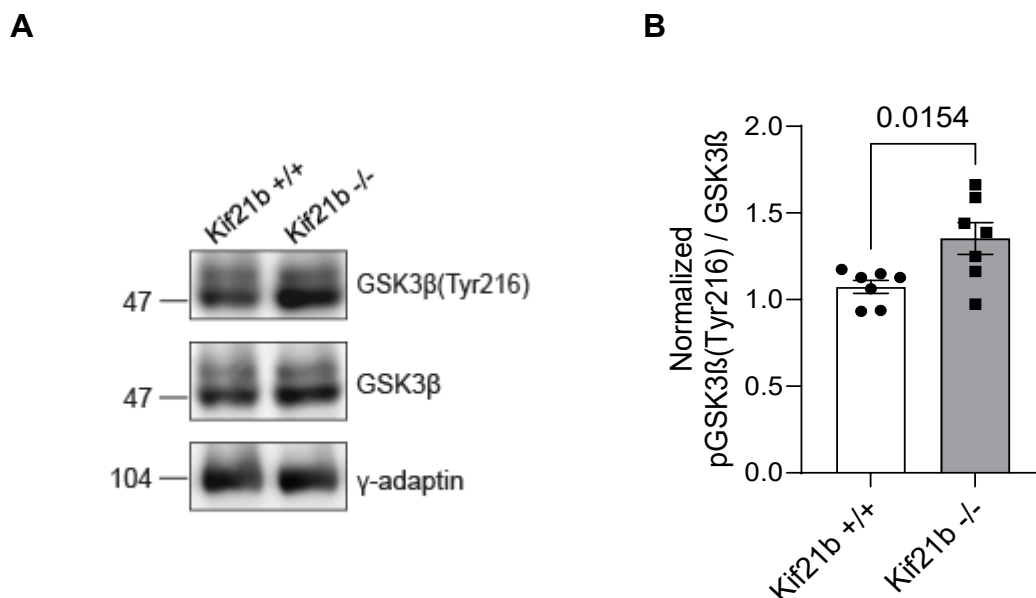


**Figure 8. Phosphorylated GSK3 $\beta$  (Tyr216) is increased in Kif21b  $-/-$  mice**



**A.** Western blot was performed to assess GSK3 $\beta$  (Tyr216) (the lower band) in brain lysates obtained from 41-42 week-old Kif21b +/+ mice and Kif21b -/- mice. GSK3 $\beta$  (Tyr216) and total GSK3 $\beta$  levels were detected, with  $\gamma$ -adaplin as the loading control.  
**B.** The intensity of phosphorylated GSK3 $\beta$  (Tyr216) was quantified using GSK3 $\beta$  (Tyr216) and normalized to total GSK3 $\beta$  levels as depicted in (A). n = 7 mice per genotype. Statistical P value was determined using a two-sided unpaired Student's t-test. The data are shown as mean  $\pm$ SEM.

#### **4.4 The role of KIF21B knockout on phosphorylated Tau at the phenotypic level**

A marked elevation in phosphorylated Tau levels was observed in the brain lysate of Kif21b -/- mice. To validate this finding, cortical brain slices from KIF21B knockout (KO) mice and wild-type (WT) mice were stained using the phosphorylated Tau-specific antibody AT8.

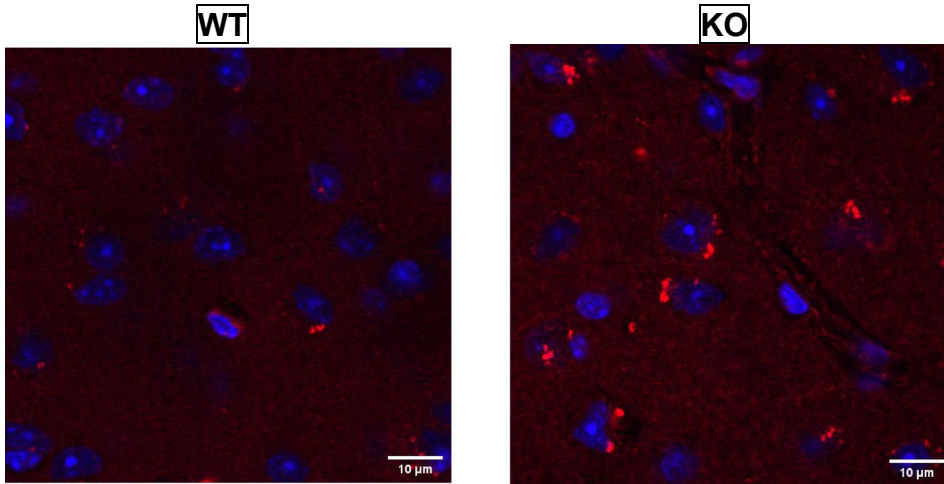
Examination of phosphorylated Tau levels in neuronal somata at higher magnification showed pronounced phosphorylation in perinuclear regions of KIF21B KO model cells, which was much lower than the level found in cells from WT mice (Figure 9A).

Comparatively, the KIF21B KO mice exhibited a significantly higher number of AT8 clusters per image area when normalized ( $p=0.0252$ ), along with significantly larger normalized AT8 cluster sizes ( $p=0.0034$ ) and a significant increase in normalized integrated intensity per AT8 cluster size ( $p=0.0490$ ) (Figure 9B-D).

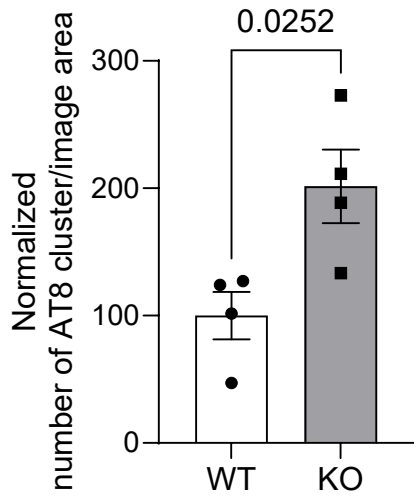
However, in both KIF21B KO mice and WT mice, no significant differences were observed in the normalized pan Tau-positive cell area, normalized pan Tau average intensity per cell, and normalized pan Tau integrated intensity per cell (Figure 9E-H).

In conclusion, a significant increase in cortical sections containing phosphorylated Tau level was detected using the KIF21B knockout model compared to wild-type controls.

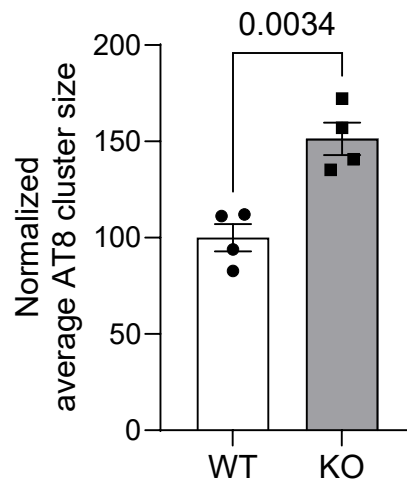
**A**



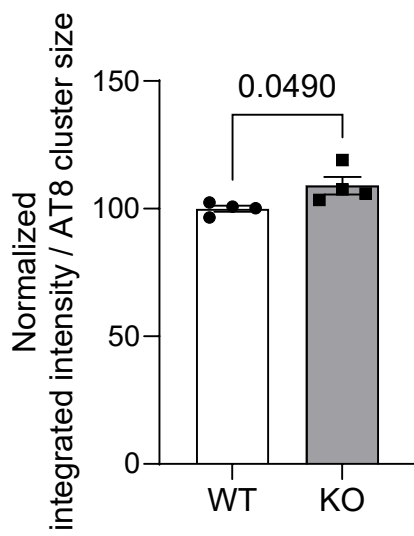
**B**

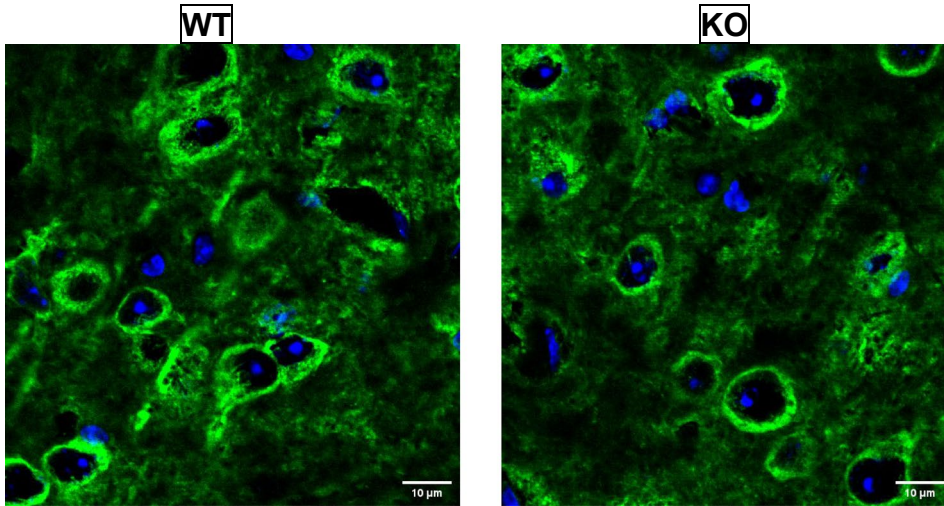
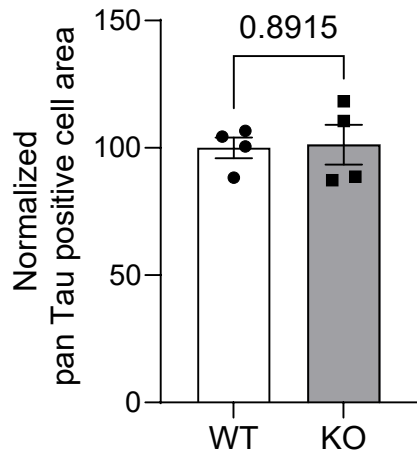
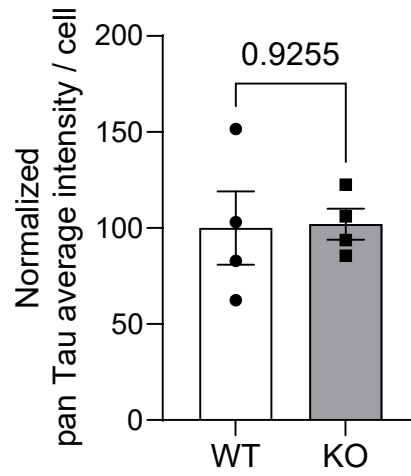
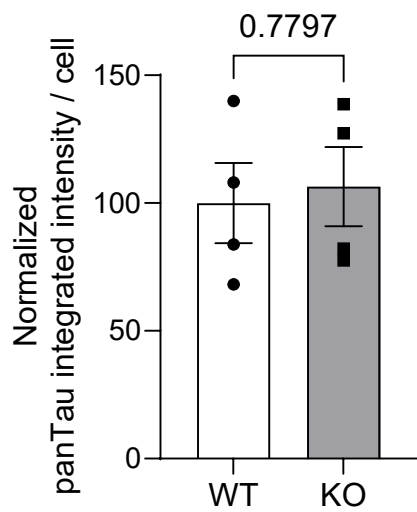


**C**



**D**



**E****F****G****H**

### **Figure 9. Elevated phosphorylated Tau phenotype in KIF21B KO mice**

**A.** Immunohistochemical analysis revealed subcellular accumulations of phosphorylated Tau in layer V of cortical brain sections obtained from 41-42 week-old WT mice and KIF21B KO mice. WT mice were used as controls. Phosphorylated Tau was labeled with AT8 (red), while nuclei were stained with DAPI (blue). Scale bar=10 $\mu$ m.

**B, C, D.** Quantification of the size of AT8-positive accumulations per analyzed area, as depicted in (A). n = 4 mice per genotype.

**E.** Immunohistochemical studies showed similar subcellular localization of Tau aggregates in the cortical brain sections of 41- to 42-week-old mice in both WT and KIF21B KO. The antibody control was obtained from the wild-type sections. Total Tau was labeled with Tau (green), while nuclei were stained with DAPI (blue). Scale bar=10 $\mu$ m.

**F, G, H.** Quantification of the size of pan Tau-positive accumulations per analyzed area (F) and signal intensities per analyzed area (G, H) as illustrated in (E). n = 4 mice per genotype. Statistical significance was determined using two-sided unpaired Student's t-tests. Data are presented as mean  $\pm$  SEM (B-D, F-H).

## **4.5 Axonal trafficking of kinesin-dependent synaptophysin in the initial stages of inflammatory triggers**

It has been demonstrated in vain that genetic variants in the KIF21B gene are associated with multiple sclerosis (MS) and other inflammatory diseases (Goris et al., 2010; Yang et al., 2015). A two-part investigation can be conducted to understand the involvement of KIF21B in multiple sclerosis.

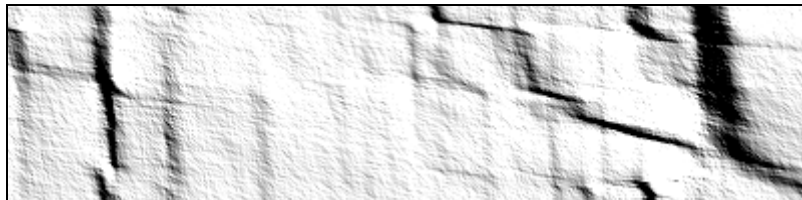
The first part is that after Mouse cortical neurons cultured in vitro (DIV) for 12 days and co-transfected with target protein plasmids (Synaptophysin-GFP, mCherry-BDNF, N-cadherin-RFP, Lamp1-RFP) and volume markers (GFP or Ruby) for 6 hrs, a chronic inflammation cocktail (IC) was simultaneously used or not (INF-Gamma, TNF- $\alpha$ , IL17, 100 nM each), using IC as the treatment group and none as the non-treatment group. Then, cortical neurons were incubated at 37°C in an incubator with 5% CO<sub>2</sub> for 48 hours. Nikon spinning disk imaging system in 37°C and 5% CO<sub>2</sub>-controlled mode from our lab was used. Volume markers identified axons as axons that differ morphologically from dendrites, and live-cell imaging of neurons expressing the target protein cargoes allowed the observation of bidirectional axonal transport of the target protein cargoes.

Secondly, the role of KIF21B in inflammation will be extensively investigated in the future, focusing on its effect on inflammation-induced bidirectional transport of cargo within axons. It will involve the study of the bidirectional transport of cargoes within

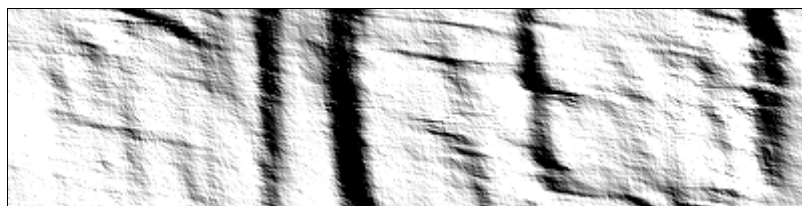
axons of KIF21B knockout (KO) cortical neurons after 48 hours of exposure to an inflammatory cocktail compared to wild-type neurons. The inflammatory cocktail will be used again to assess bidirectional cargo transport in axons of KIF21B KO versus WT cortical neurons in the early stages of neuroinflammation.

The axonal transport of synaptophysin is suggested to depend on KIF1A (Okada et al., 1995). To clarify the axonal transport of KIF1A-dependent synaptophysin in the initial stages of inflammatory Triggers, mouse cortical neurons were cultured in vitro (DIV) for 12 days and co-transfected with Synaptophysin-GFP and volumetric markers, Ruby. After 6 hours, neurons were treated with or without an IC containing INF-Gamma, TNF-alpha, and IL17, each at a concentration of 100 nM. The neurons were incubated for 48 hours. Rates in different directions and the number of particles in different states were compared between conditions after 48 hours with or without inflammatory stimuli. The comparison revealed no significant differences in the velocity of anterograde and retrograde axonal transport (Figure 10A-F). Specifically, no notable variances were observed in the transport of particles in either direction or the number of stationary particles (Figure 10G-H). These observations suggest that the axonal transport of synaptophysin remains largely unchanged during the initial phase of inflammatory stimulation.

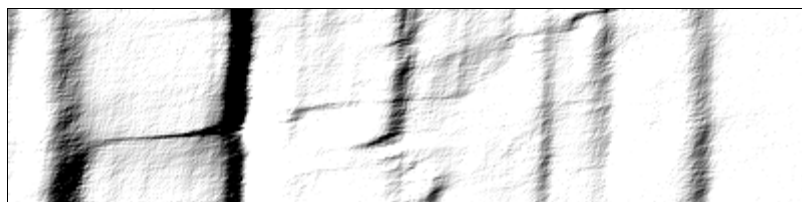
**A**



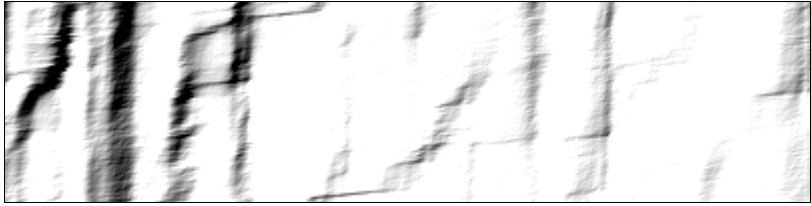
Non-treatment, anterograde



Treatment, anterograde

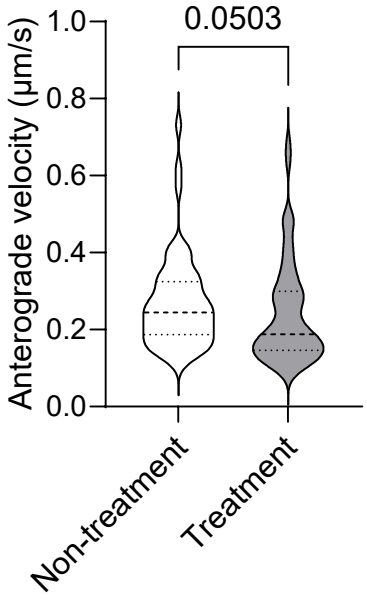


Non-treatment, retrograde

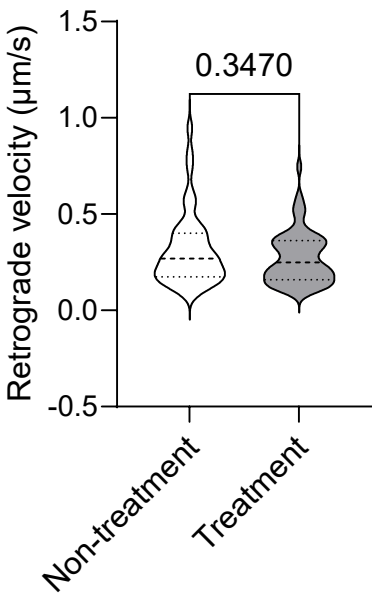


Treatment, retrograde

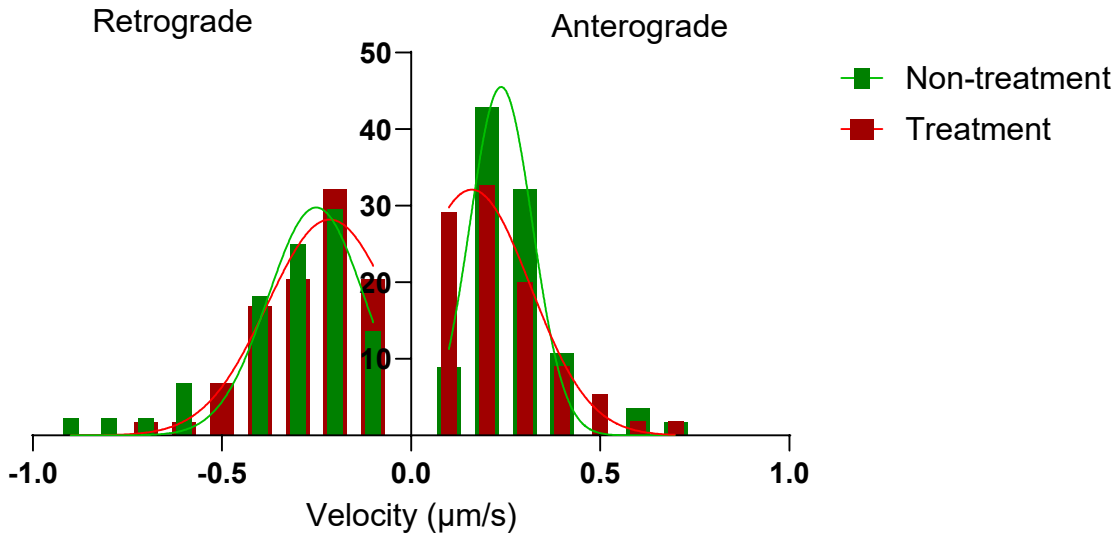
**B**



**C**



**D**



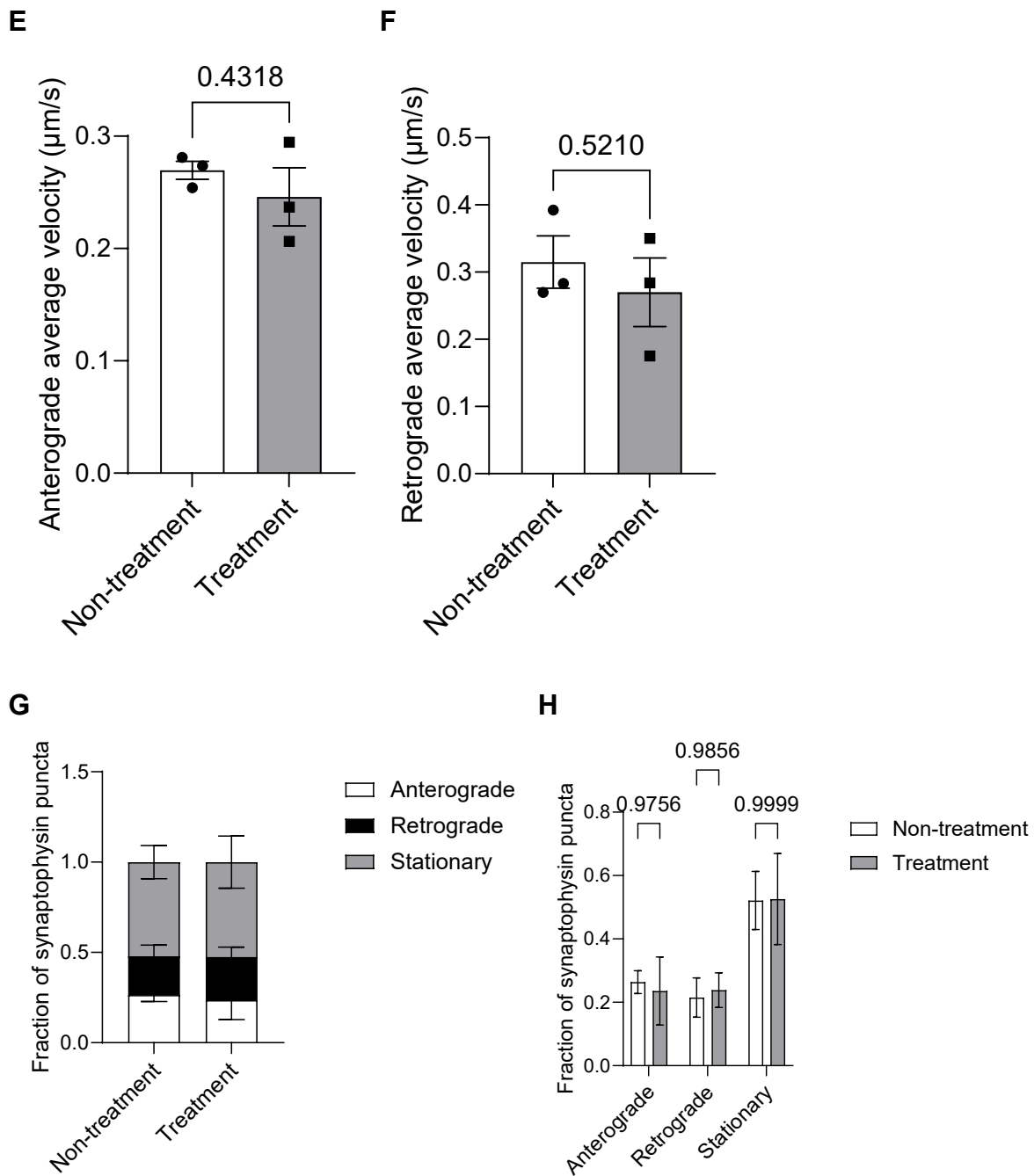


**Figure 10. Axonal trafficking of synaptophysin in the initial stages of inflammation**

**A.** Kymographs depicting Synaptophysin-GFP motility in 12-day in vitro (DIV) cortical neuron axons were generated with or without inflammation treatment for 48 hours. Sample events are traced below the kymographs.

**B, C.** The run velocity of all motile Synaptophysin-GFP puncta in the anterograde and retrograde directions was analyzed. The sample size consisted of  $n = 15-18$  neurons per condition. Statistical significance was determined using a Mann-Whitney test. The data are presented as mean  $\pm$  SEM.

**D.** Histograms were created to display the transport velocities of Synaptophysin-GFP particles based on data from 15-18 cells.

**E, F.** The average run velocity of motile Synaptophysin-GFP puncta in the anterograde and retrograde directions was calculated across three independent experiments ( $n =$

3). Statistical significance was determined using two-sided unpaired a Student's t-test. The data are presented as mean  $\pm$  SEM.

**G, H.** The fraction of anterograde, stationary, and retrograde Synaptophysin-GFP puncta was determined using Two-way ANOVA for statistical analysis.

#### **4.6 Axonal trafficking of kinesin-dependent BDNF in the initial stages of inflammation**

It has been shown that axonal transport of BDNF is also dependent on the KIF5C motor (Hirokawa et al., 2010). To elucidate the KIF5C-dependent axonal transport of BDNF during the initial stages of trigger inflammation, mouse cortical neurons were cultured in DIV12 and co-transfected with mCherry-BDNF and GFP. After 6 hours, neurons were treated (48 hours) with or without IC containing INF- $\gamma$ , TNF- $\alpha$ , and IL17 (at concentrations of 100 nM each). The rates in different directions and the number of particles in various states were evaluated under inflammatory conditions at 48 hours.

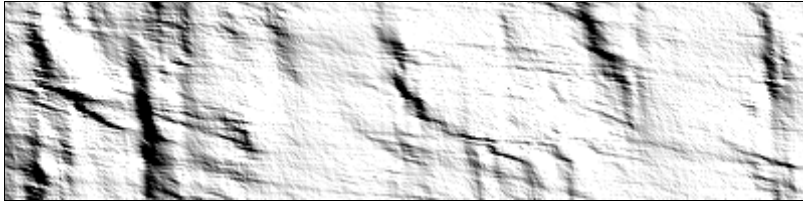
It was observed that with an inflammatory stimulus, the anterograde transport of all mCherry-BDNF particles was significantly decelerated compared to the group without an inflammatory stimulus ( $p=0.0045$ ). However, there was no significant alteration in the velocity of retrograde transport (Figure 11A-D). These findings imply a potential influence on the kinesin regulating the axonal transport of mCherry-BDNF during the initial phase of inflammatory stimulation. Nevertheless, in the average experiment involving  $n = 3$ , no notable discrepancy in the rates of anterograde and retrograde transport was observed, suggesting that more repetitions of experiments are needed (Figure 11E-F). Furthermore, no significant differences were observed between anterograde, retrograde, and stationary particles with or without inflammatory stimuli over 48 hours (Figure 11G-H). Within this study's scope, there appears to be no notable impact on the axonal transport of BDNF during the early stages of inflammatory stimulation. However, nuances may necessitate elucidation through additional experimentation involving a broader array of samples.



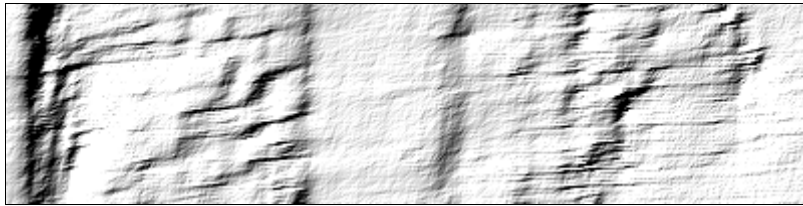
**A**



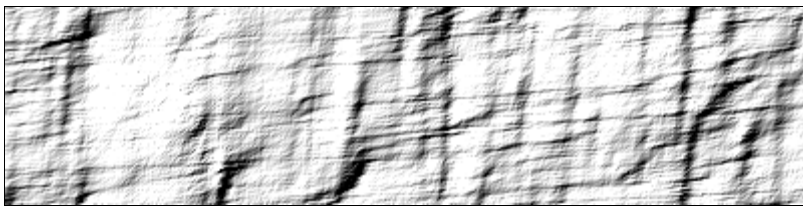
Non-treatment,anterograde



Treatment, anterograde

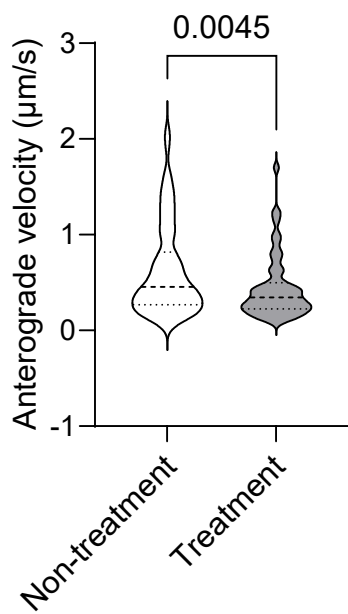


Non-treatment, retrograde

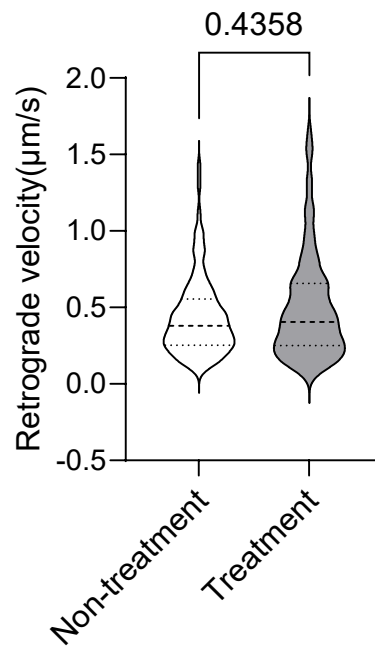


Treatment, retrograde

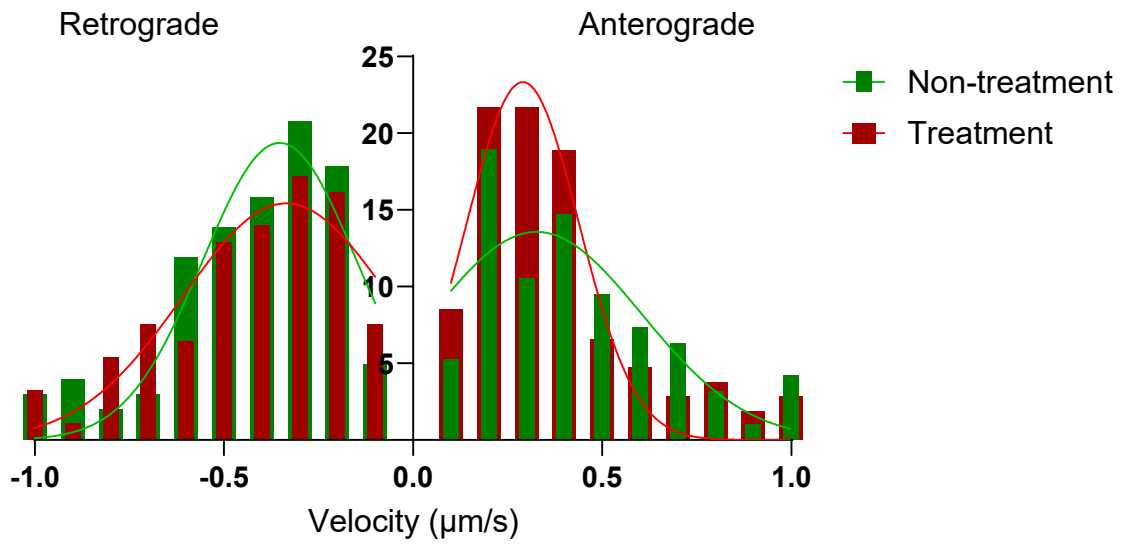
**B**



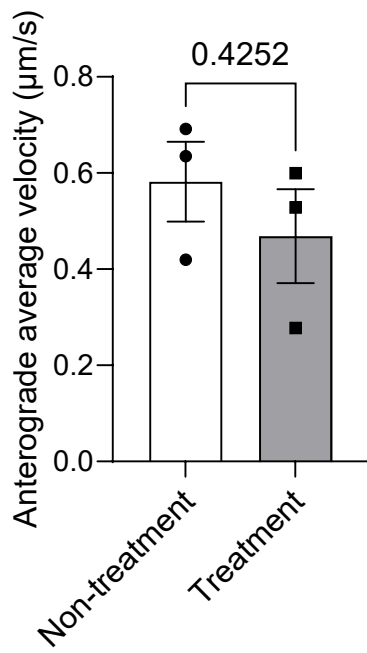
**C**



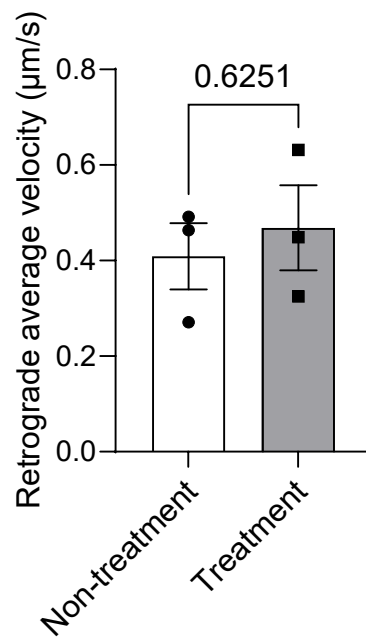
D



E



F



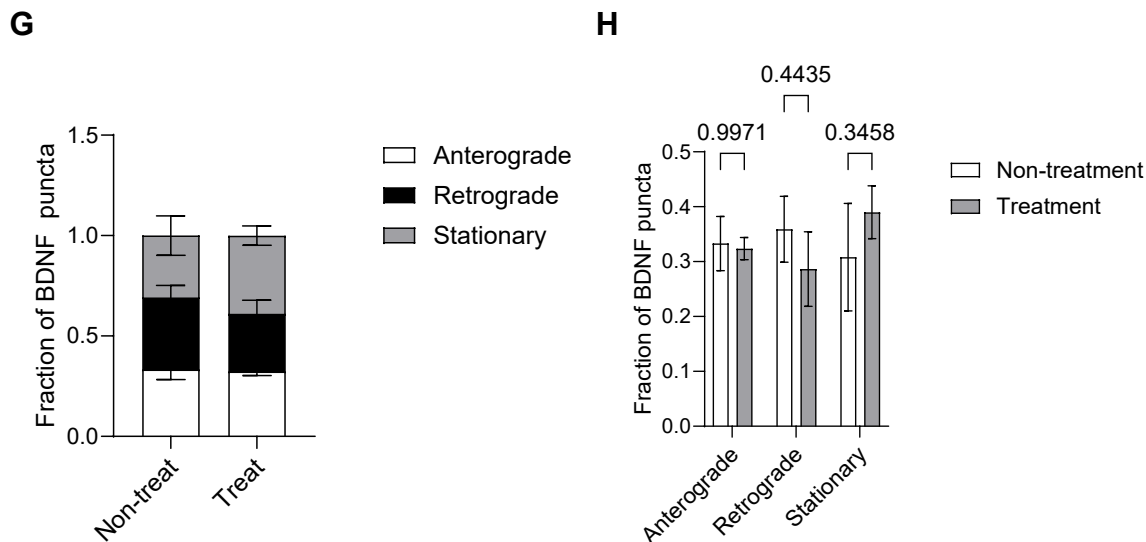


**Figure 11. Axonal trafficking of BDNF in the initial stages of inflammation**

**A.** Kymographs illustrating the motility of mCherry-BDNF in DIV12 cortical neuron axons were generated with or without inflammation treatment for 48 hours. Sample events are traced below the kymographs.

**B, C.** The run velocity of all motile mCherry-BDNF puncta was evaluated, with a sample size of  $n = 15-18$  neurons per condition. Statistical significance was assessed using a Mann-Whitney test. The data are presented as mean  $\pm$  SEM.

**D.** Histograms were constructed to illustrate the transport velocities of mCherry-BDNF particles derived from data collected from 15-18 neurons.

**E, F.** Three independent experiments ( $n = 3$ ) determined the average run velocity of motile mCherry-BDNF puncta. Statistical significance was determined using an unpaired Student's t-test with two-sided analysis. Data are represented as mean  $\pm$  SEM.

**G, H.** Two-way ANOVA analyzed the fractional representation of anterograde, stationary, and retrograde mCherry-BDNF puncta.

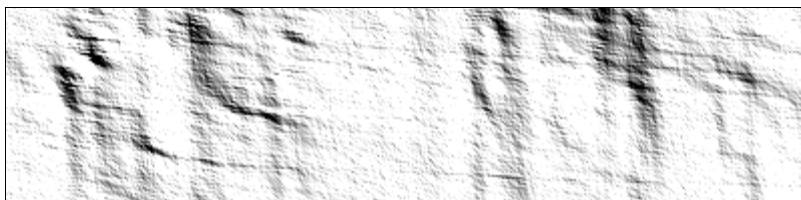
#### 4.7 Axonal trafficking of kinesin-dependent N-cadherin in the initial stages of inflammatory triggers

It has been shown that axonal transport of N-cadherin also depends on the KIF3A motor (Shima et al., 2007). To elucidate what changes occur in the bidirectional axonal transport of KIF3A-dependent N-cadherin during the initial phase of induced inflammation, mouse cortical neurons were cultured in DIV12 and co-transfected with N-cadherin-RFP and GFP. 6 hr later, neurons were treated (48 h) with or without ICs containing INF- $\gamma$ , TNF- $\alpha$ , and IL17 (100 nM each). The rates in different directions and

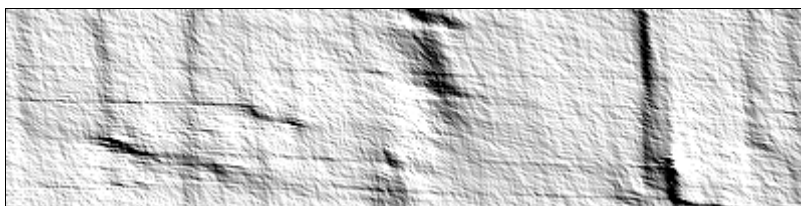
the number of particles in various states were measured under inflammatory conditions at 48 hours.

Interestingly, under inflammatory conditions, the retrograde transport velocity of all N-cadherin-RFP particles was significantly reduced compared to the group without inflammatory stimulus ( $p=0.0183$ ). At the same time, no significant difference was observed in the anterograde transport velocity (Figure 12A-D). These findings suggest that the axonal transport of N-cadherin may be more influenced by dynein's role during the initial phase of inflammatory triggering. However, across the three experiments conducted ( $n=3$ ), there remained no significant disparity between the anterograde and retrograde transport velocities, suggesting that more repetitions of experiments are needed (Figure 12E-F). Furthermore, no significant differences were observed in the proportions of anterograde, retrograde, and stationary particles during the 48 hours with and without inflammatory stimuli (Figure 12G-H). The outcomes indicate that, during the initial phase of inflammatory triggering, there appears to be no substantial influence on the axonal transport of N-cadherin. These subtle differences, however, may have to be demonstrated by more extensive experiments in a broader range of samples.

**A**



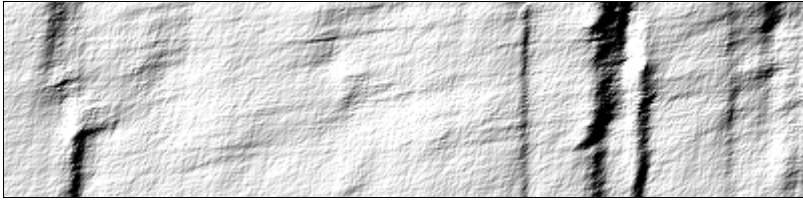
Non-treatment, anterograde



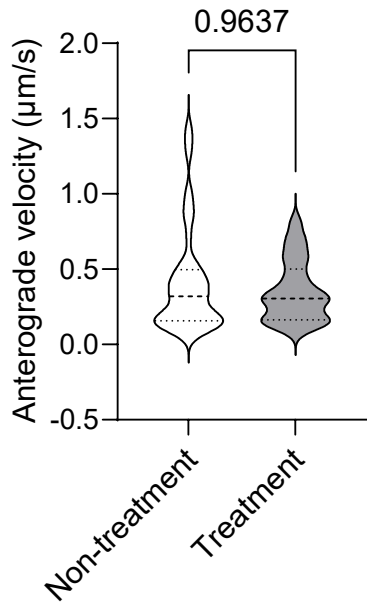
Treatment, anterograde



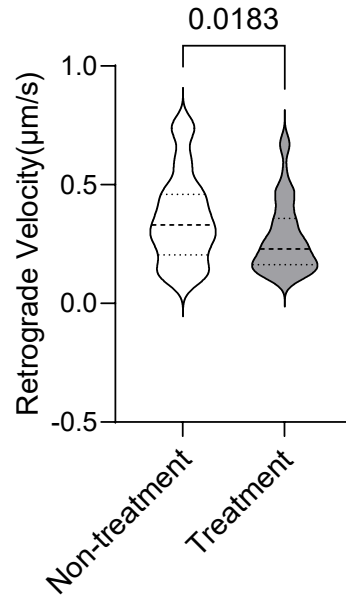
Non-treatment, retrograde



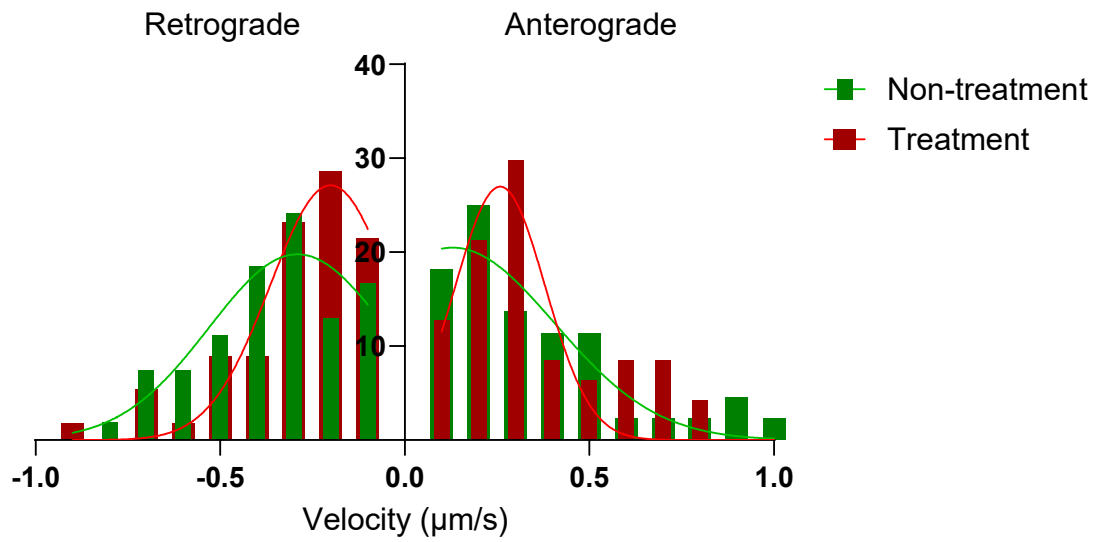
**B**



**C**



**D**



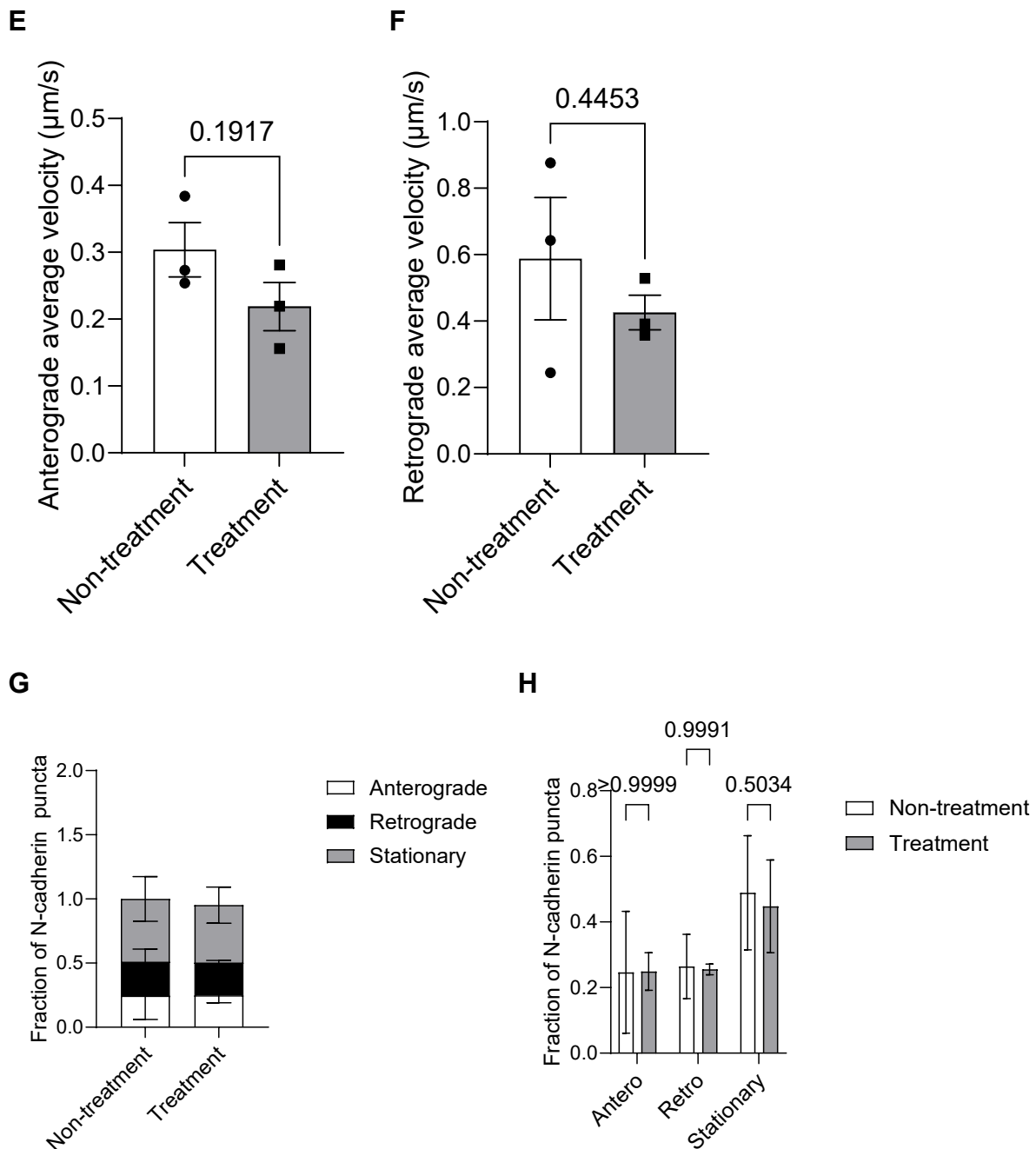


**Figure 12. Axonal trafficking of N-Cadherin in the initial stages of inflammation**

**A.** Kymographs illustrating the motility of N-cadherin-RFP in DIV12 cortical neuron axons were generated with or without inflammation treatment for 48 hours. Sample events are traced below the kymographs.

**B, C** Analysis of the run velocity for all motile N-cadherin-RFP puncta was conducted, with a sample size of  $n = 15-18$  neurons per condition. Statistical significance was determined using a Mann-Whitney test. The data are presented as mean  $\pm$  SEM.

**D.** Histograms were prepared to present the distribution of transport velocities of N-cadherin-RFP particles based on data collected from 15-18 cells.

**E, F** The average run velocity of motile N-cadherin-RFP puncta across three experimental replicates ( $n = 3$ ) was calculated. Statistical significance was determined using a two-sided unpaired Student's t-test. The data are presented as mean  $\pm$  SEM.

**G, H** The fractional representation of anterograde, stationary, and retrograde N-cadherin-RFP puncta was analyzed using Two-way ANOVA for statistical analysis.

#### **4.8 Axonal trafficking of dynein-dependent LAMP1 in the initial stages of inflammation**

LAMP1 (Lysosome-associated membrane protein 1) is a transmembrane protein primarily located in lysosomes and plays a crucial role in lysosomal function and neuronal health (Saftig and Klumperman, 2009; Nakanishi, 2015). The axonal transport of N-cadherin is suggested depending on the dynein (Harada et al., 1998). To investigate the impact of initial inflammatory stimuli on the dynein-dependent axonal transport of LAMP1, mouse cortical neurons were cultured in DIV12 and co-transfected with Lamp1-RFP and GFP. After 6 hours, neurons were treated (48 hours) with or without IC containing INF- $\gamma$ , TNF- $\alpha$ , and IL17 (100 nM each). The rates in different directions and the number of particles in various states were evaluated with or without inflammatory conditions at 48 hours.

It was observed that under inflammatory conditions, the retrograde transport velocity of all Lamp1-RFP particles was significantly lower than that of the group without an inflammatory stimulus ( $p=0.0014$ ). At the same time, there was no significant difference in the anterograde transport velocity (Figure 13A-D). These findings suggest that dynein, which regulates retrograde axonal transport of LAMP1, may be affected during the initial phase of inflammatory triggering. However, retrograde and anterograde transport velocities still showed no significant differences in the average experiments ( $n=3$ ) (Figure 13E-F). Likewise, no significant differences were observed between anterograde particles, retrograde particles, and stationary particles during the 48 hours with or without inflammatory stimuli, suggesting that more repetitions of experiments are needed (Figure 13G-H). In aggregate, the investigation indicates that, within its parameters, there is no discernible effect on the axonal transport of LAMP1 during the initial phases of inflammatory stimulation. Nonetheless, further investigation employing a more extensive range of samples may uncover subtle nuances warranting clarification.

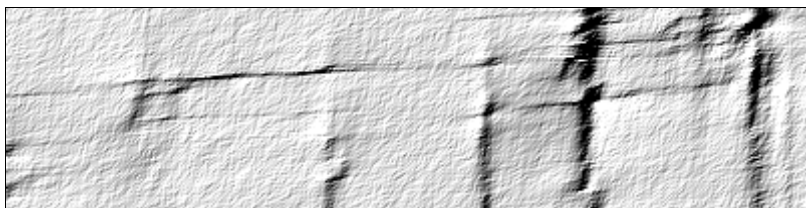
**A**



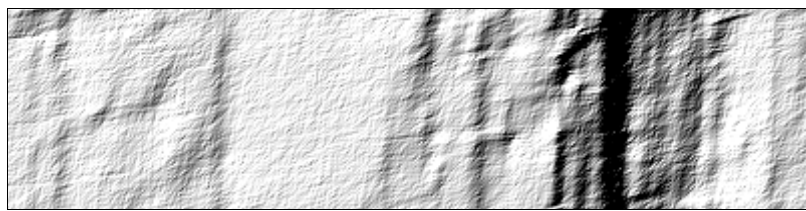
Non-treatment, anterograde



Treatment, anterograde

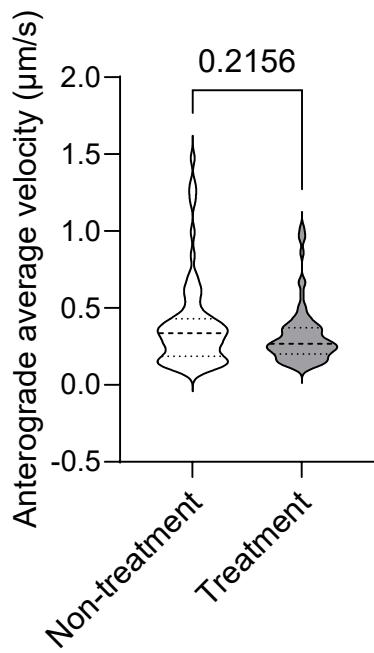


Non-treatment, retrograde

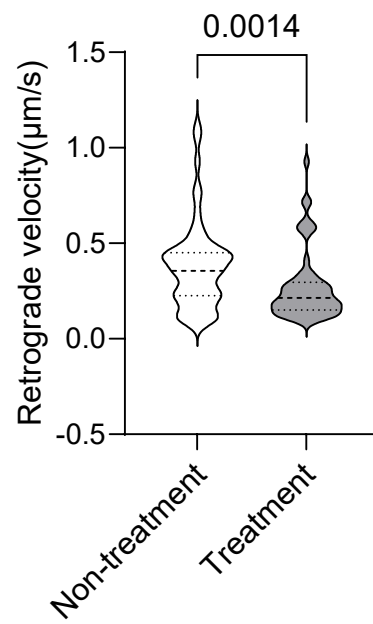


Treatment, retrograde

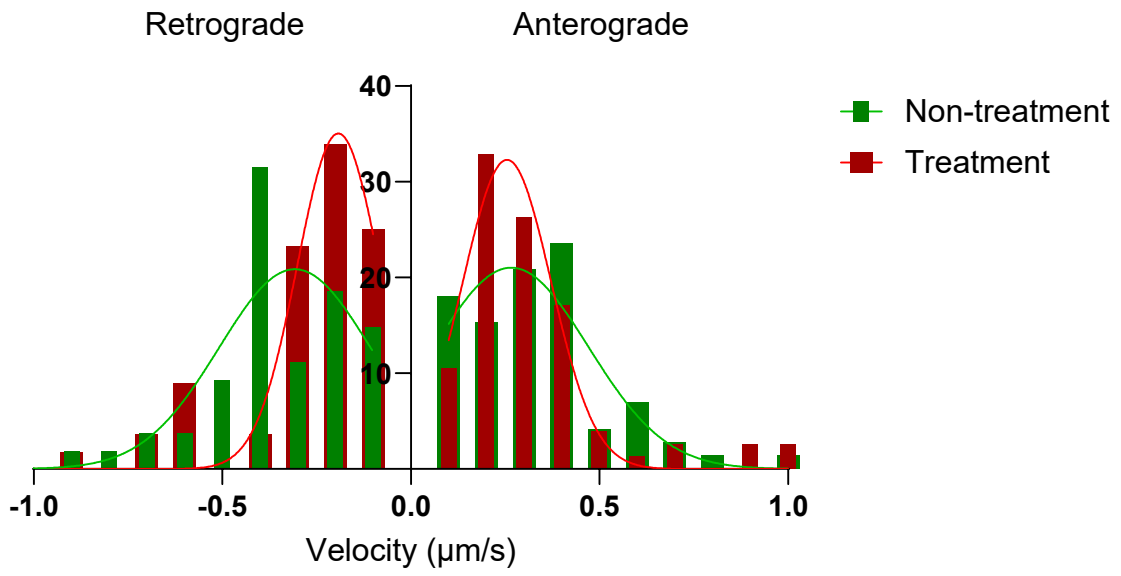
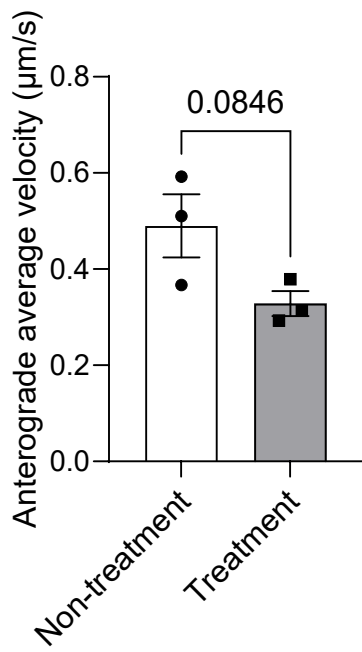
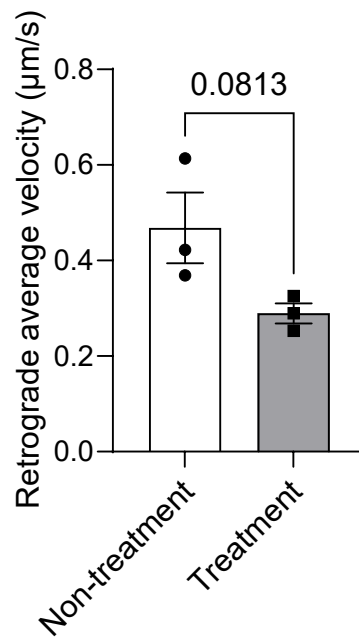
**B**



**C**





**D****E****F**

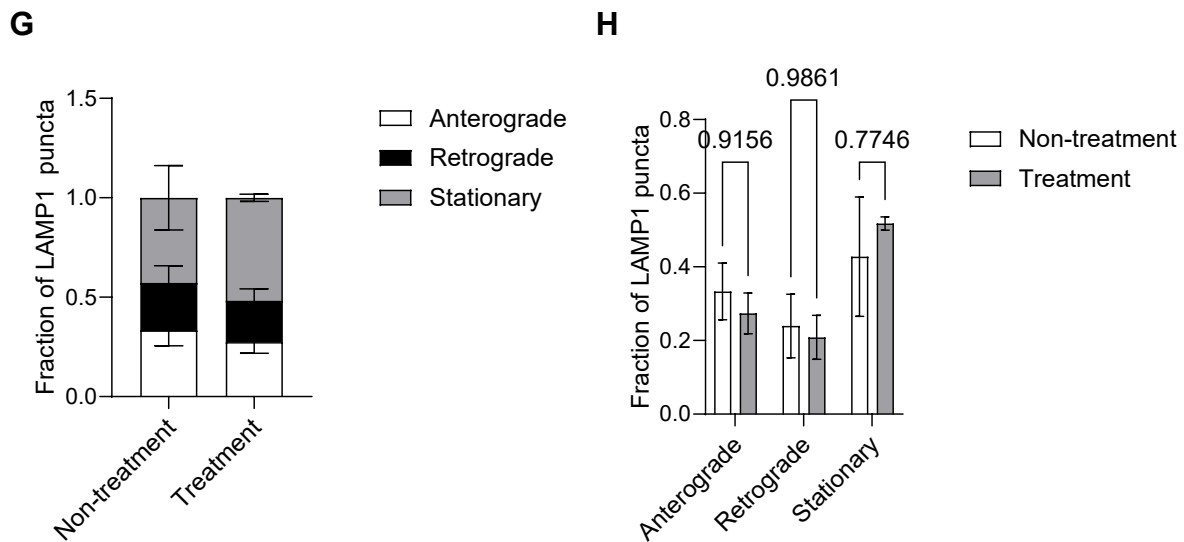


**Figure 13. Axonal trafficking of LAMP1 in the initial stages of inflammation**

**A.** Kymographs depicting the motility of Lamp1-RFP in 12-day in vitro (DIV) control cortical neuron axons were generated, both with and without inflammation treatment, for 48 hours. Representative events are annotated below the kymographs.

**B, C.** The evaluation of the run velocity of all motile Lamp1-RFP puncta was performed, involving 15-18 neurons per condition. Statistical significance was determined using a Mann-Whitney test. The data are presented as mean  $\pm$  SEM.

**D, E.** It represents the quantification of the average run velocity of motile Lamp1-RFP puncta, and data are represented as mean  $\pm$  SEM across three independent experiments ( $n = 3$ ). Statistical significance was considered by using the two-sided unpaired Student's t-test.

**F.** Histograms illustrating the transport velocities of Lamp1-RFP particles, based on data collected from 15-18 neurons.

**G, H.** Fractional representation of anterograde, stationary, and retrograde Lamp1-RFP puncta, analyzed using Two-way ANOVA.

## 5. Discussion

### 5.1 The role of KIF21B knockout on Tau phosphorylation

Here, the data show reduced phosphorylated Akt, elevated phosphorylated GSK3 $\beta$  (Tyr216), and elevated phosphorylated Tau in KIF21B knockout mice compared to wild-type by brain homogenate protein blotting experiments and immunohistochemistry in layer V of the cerebral cortex. It seems that KIF21B knockout acts reduce activation of the PI3K/Akt signaling pathway, leading to a reduction in phosphorylated Akt and, thus, to a decline in the inhibition of GSK3 $\beta$  phosphorylation. The result is an increase in phosphorylated GSK3 $\beta$  (Tyr216), which activates more Tau phosphorylation (Kreft et al., 2005; Tejada et al., 2017; Lauretti et al., 2020; Songjia et al., 2021).

KIF21B knockout can activate the PI3K/Akt signaling pathway through direct or indirect action (Songjia et al., 2021). Autophosphorylation on tyrosine-279/216 mediates GSK3 $\beta$  activation, whereas phosphorylation of serine site 21/9 by N-terminal AKT, protein kinases A and B (PKA-PKB) leads to its inhibition (Ly et al., 2013). Overactive GSK3 $\beta$  promotes phosphorylation and the formation of toxic Tau species (Phiel et al., 2003). Finally, the present study concludes that KIF21B knockout may inhibit the phosphorylation of Akt and increase GSK3 $\beta$  (Tyr216), leading to Tau's phosphorylation.

Although these studies reveal essential discoveries, there are also limitations. Firstly, this study did not explore the exact signaling pathway of the effect of KIF21B knockout on Tau phosphorylation. Second, this study used brain homogenate, not hippocampus homogenate, in protein blotting. Third, using cortical layer V in immunohistochemistry is based on previous studies showing that phosphorylated Tau expression is more significant in cortical layer V in aged rats (Hausrat et al., 2022). The present study did not explore where phosphorylated Tau expression was greater. Notwithstanding its limitation, this study does suggest that KIF21B KO contributes to an increase in the phosphorylation of Tau.

In light of these limitations, the next step in the investigation involves exploring the precise signal pathway of the effects of KIF21B knockout on Tau phosphorylation.

## 5.2 The effect of inflammatory triggers on bidirectional axonal transport of cargoes

In this study, the kinesin-dependent axonal transport of synaptophysin, BDNF, and N-cadherin and dynein-dependent LAMP1 in neurons was tracked by live-cell imaging 48 hours after inflammatory stimulation. The results show no significant differences in all statistics for N=3. No significant differences exist in anterograde kinesin-dependent, retrograde dynein-dependent, and stationary number stop comparisons for all particles. While none of the summary statistics for particle rates reached statistical significance, the velocity comparison of all particles yielded valuable insights and information for the study. The following are examples. The kinesin-dependent anterograde transport of the BDNF in the inflammation-stimulated group is significantly slower than the control group. In contrast, there is no significant difference in the dynein-dependent retrograde transport of BDNF. Interestingly, kinesin-dependent N-cadherin is not considerably different in anterograde transport and is markedly slower in dynein-dependent retrograde transport in the treatment group than in the non-treatment group. Dynein-dependent LAMP1 is significantly slower in retrograde transport in the inflammation-stimulated group than in the control group, with no significant difference in kinesin-dependent anterograde transport.

In multiple sclerosis (MS), extensive transporter impairment and reduced availability of distal organelles such as mitochondria may lead to axonal atrophy late in the disease (Sorbara et al., 2014). This study further explores the specific dynamics affected at the onset of inflammation. Axonal transport of LAMP1, BDNF, and synaptophysin has been explored, with KIF1A primarily acting on synaptophysin and KIF5C mostly on BDNF (Okada et al., 1995; Hirokawa et al., 2010), showing that KIF1/kinesin-3, but not KIF5/kinesin-1, mediates signaling-dependent transporter selectivity (Tymanskyj et al., 2022). The findings of this study indicate that cargo transport remains unaffected at the initiation of inflammatory stimuli when the experiment was conducted with n=3. However, an analysis of all particles rate results suggests that synaptophysin may modestly impede retrograde transport, albeit not significantly. At the same time, BDNF, potentially impacted by KIF5C damage, significantly retards the anterograde transport of all particles. Notably, N-cadherin appears to be more influenced by dynein, as does LAMP1. In summary, these results suggest no discernible effect on cargo axonal

transport during the early phases of inflammatory stimulation. It is conceivable that alterations in axonal transport kinetics could affect cargo axonal transport, but further experiments with a larger sample size are warranted to substantiate these observations.

The obvious shortcoming of this experiment is that there is no significant difference in all the results if N=3. In contrast, there is a substantial difference in the results when all the particles are taken. The sample size needs to be increased, and one to two more experiments will be conducted to confirm the difference in the results. Again, all the particle velocity results of this study are informative.

The next step is to do a few more experiments to confirm the variability of the results in the inflammation wild-type model. To further explore the involvement of KIF21B in inflammation compared to WT neurons, the focus will be on KIF21B KO cortical neurons. Following transfection with kinesin-dependent synaptophysin, BDNF, and N-cadherin, these neurons will be subjected to an inflammatory cocktail (IC) for 48 hours. Similarly, the inflammatory cocktail will be utilized to study the retrograde movement of LAMP1 in KIF21B KO versus WT cortical axons.

## 6. Conclusion

In conclusion, The first part of this study investigated KIF21B knockout decrease phosphorylated Akt and subsequently increase of GSK3 $\beta$ (Tyr216) activation, which might lead to increased phosphorylated Tau levels, suggesting that KIF21B may influence the activation of the PI3K/Akt signaling pathway, which subsequently inhibits the phosphorylation of GSK3 $\beta$ (Tyr216) and thus suppresses Tau phosphorylation in physiological condition. Future studies address this gap and conduct rescue experiments. In summary, the study highlights the potential role of KIF21B in the pathogenesis of Alzheimer's disease, in which KIF21B within the PI3K/Akt/ GSK3 $\beta$  pathway may offer novel therapeutic strategies for treating Alzheimer's disease.

The second part of this study suggests that kinesin-dependent synaptophysin, BDNF, N-cadherin, and dynein-independent LAMP1 do not exhibit significant differences in the wild-type model of neuroinflammation for 48 hours compared to wild-type cortical neurons. However, some results regarding the velocity of all protein particles indicate potential effects, possibly due to insufficient sample size. More extensive experiments in a broader range of samples may demonstrate these subtle differences. Additionally, further research will explore the bidirectional axonal transport of protein-dependent and protein-independent cargoes influenced by KIF21B KO during neuroinflammation within 48 hours.

## 7. List of abbreviations

AD	Alzheimer's disease
A $\beta$	Amyloid beta
NFTs	Neurofibrillary tangles
APP	Amyloid precursor protein
PHFs	Paired helical filaments
MAP	Microtubule-associated protein
MTs	Microtubules
CNS	Central nervous system
NGF	Nerve growth factor
NT-3	Neurotrophin-3
PLC $\gamma$	Phospholipase C gamma
IP <sub>3</sub>	Inositol trisphosphate
JNK	c-Jun N-terminal kinase
ERK	Extracellular Signal-Regulated Kinase
PI3K	Phosphoinositide 3-kinase
GSK3 $\beta$	Glycogen Synthase Kinase 3 $\beta$
PKA	Protein kinase A
Akt (PKB)	Protein kinase B
KIFs	Kinesin superfamily proteins
KIF21A	Kinesin family member 21A
KIF21B	Kinesin family member 21B
KHC	Kinesin Heavy Chain
OS	Osteosarcoma
NDC	Non-demented controls
MS	Multiple sclerosis
OLG	Oligodendrocytes
EAE	Experimental Autoimmune Encephalomyelitis
CFA	Complete Freund's adjuvant
MOG35–55	Myelin oligodendrocyte glycoprotein 35– 55
DCs	Peripheral dendritic cells
Th1	T helper 1
IL-12	Interleukin-12
MIP-1	Macrophage inflammatory protein-1
APCs	Antigen-presenting cells
CKs	Cytokines
ES	Embryonic stem
PFA	Paraformaldehyde
PNGM	Primary Neuron Growth Medium
CaCl <sub>2</sub>	Calcium chloride
BSA	Bovine Serum Albumin
DAPI	4',6-diamidino-2-phenylindole
DH5 alpha	Douglas Hanahan5-alpha
SDS	Sodium dodecyl sulfate
PMSF	Phenylmethylsulfonyl fluoride
IC	Inflammatory cocktail
DIV	Day in vitro
SEM	Standard error of the mean

LAMP1	Lysosome-Associated Membrane Protein 1
IFN- $\gamma$	Interferon-gamma
TNF- $\alpha$	Tumor Necrosis Factor-alpha
rmIL-17	Recombinant mouse interleukin-17



## 8. References

- Alonso AC, Grundke-Iqbal I, Iqbal K. Alzheimer's disease hyperphosphorylated tau sequesters normal tau into tangles of filaments and disassembles microtubules. *Nat Med*. 1996 Jul;2(7):783-7. doi: 10.1038/nm0796-783. PMID: 8673924.
- Brunet A, Datta SR, Greenberg ME. Transcription-dependent and -independent control of neuronal survival by the PI3K-Akt signaling pathway. *Curr Opin Neurobiol*. 2001 Jun;11(3):297-305. doi: 10.1016/s0959-4388(00)00211-7. PMID: 11399427.
- Carrillo-Mora P, Luna R, Colín-Barenque L. Amyloid beta: multiple mechanisms of toxicity and only some protective effects? *Oxid Med Cell Longev*. 2014;2014:795375. doi: 10.1155/2014/795375. Epub 2014 Feb 5. PMID: 24683437; PMCID: PMC3941171.
- Cason SE, Holzbaur ELF. Selective motor activation in organelle transport along axons. *Nat Rev Mol Cell Biol*. 2022 Nov;23(11):699-714. doi: 10.1038/s41580-022-00491-w. Epub 2022 May 30. PMID: 35637414.
- Chen LM, Xiong YS, Kong FL, Qu M, Wang Q, Chen XQ, Wang JZ, Zhu LQ. Neuroglobin attenuates Alzheimer-like tau hyperphosphorylation by activating Akt signaling. *J Neurochem*. 2012 Jan;120(1):157-64. doi: 10.1111/j.1471-4159.2011.07275.x. Epub 2011 May 13. PMID: 21496024.
- Dawson HN, Cantillana V, Jansen M, Wang H, Vitek MP, Wilcock DM, Lynch JR, Laskowitz DT. Loss of tau elicits axonal degeneration in a mouse model of Alzheimer's disease. *Neuroscience*. 2010 Aug 11;169(1):516-31. doi: 10.1016/j.neuroscience.2010.04.037. Epub 2010 Apr 29. PMID: 20434528; PMCID: PMC2900546.
- DeTure MA, Dickson DW. The neuropathological diagnosis of Alzheimer's disease. *Mol Neurodegener*. 2019 Aug 2;14(1):32. doi: 10.1186/s13024-019-0333-5. PMID: 31375134; PMCID: PMC6679484.
- Di Carlo M, Giacomazza D, San Biagio PL. Alzheimer's disease: biological aspects, therapeutic perspectives and diagnostic tools. *J Phys Condens Matter*. 2012 Jun 20;24(24):244102. doi: 10.1088/0953-8984/24/24/244102. Epub 2012 May 18. PMID: 22595372.
- Dobson R, Giovannoni G. Multiple sclerosis - a review. *Eur J Neurol*. 2019 Jan;26(1):27-40. doi: 10.1111/ene.13819. Epub 2018 Nov 18. PMID: 30300457.
- Dubey J, Ratnakaran N, Koushika SP. Neurodegeneration and microtubule dynamics: death by a thousand cuts. *Front Cell Neurosci*. 2015 Sep 9;9:343. doi: 10.3389/fncel.2015.00343. Erratum in: *Front Cell Neurosci*. 2016;10:26. PMID: 26441521; PMCID: PMC4563776.
- Engelhardt B, Comabella M, Chan A. Multiple sclerosis: Immunopathological heterogeneity and its implications. *Eur J Immunol*. 2022 Jun;52(6):869-881. doi: 10.1002/eji.202149757. Epub 2022 May 6. PMID: 35476319; PMCID: PMC9324211.
- Fahnestock M, Marchese M, Head E, Pop V, Michalski B, Milgram WN, Cotman CW. BDNF increases with behavioral enrichment and an antioxidant diet in the aged dog. *Neurobiol Aging*. 2012 Mar;33(3):546-54. doi: 10.1016/j.neurobiolaging.2010.03.019. Epub 2010 May 5. PMID: 20447733; PMCID: PMC2935515.
- Fan L, Mao C, Hu X, Zhang S, Yang Z, Hu Z, Sun H, Fan Y, Dong Y, Yang J, Shi C, Xu Y. New Insights Into the Pathogenesis of Alzheimer's Disease. *Front Neurol*. 2020 Jan 10;10:1312. doi: 10.3389/fneur.2019.01312. PMID: 31998208; PMCID: PMC6965067.

- Frost B, Jacks RL, Diamond MI. Propagation of tau misfolding from the outside to the inside of a cell. *J Biol Chem*. 2009 May 8;284(19):12845-52. doi: 10.1074/jbc.M808759200. Epub 2009 Mar 11. PMID: 19282288; PMCID: PMC2676015.
- Ghiretti AE, Thies E, Tokito MK, Lin T, Ostap EM, Kneussel M, Holzbaur ELF. Activity-Dependent Regulation of Distinct Transport and Cytoskeletal Remodeling Functions of the Dendritic Kinesin KIF21B. *Neuron*. 2016 Nov 23;92(4):857-872. doi: 10.1016/j.neuron.2016.10.003. Epub 2016 Nov 3. PMID: 27817978; PMCID: PMC5283298.
- George EK, Reddy PH. Can Healthy Diets, Regular Exercise, and Better Lifestyle Delay the Progression of Dementia in Elderly Individuals? *J Alzheimers Dis*. 2019;72(s1):S37-S58. doi: 10.3233/JAD-190232. PMID: 31227652.
- Gilley J, et al. Age-dependent axonal transport and locomotor changes and tau hypophosphorylation in a "P301L" tau knockin mouse. *Neurobiol Aging*. 2012;33(3):621.e1-621.e15
- Goris A, Boonen S, D'hooghe MB, Dubois B. Replication of KIF21B as a susceptibility locus for multiple sclerosis. *J Med Genet*. 2010 Nov;47(11):775-6. doi: 10.1136/jmg.2009.075911. Epub 2010 Jun 28. PMID: 20587413.
- Graber JJ, Dhib-Jalbut S. Protective autoimmunity in the nervous system. *Pharmacol Ther*. 2009 Feb;121(2):147-59. doi: 10.1016/j.pharmthera.2008.10.001. Epub 2008 Nov 1. PMID: 19000712.
- Grundke-Iqbal I, Iqbal K, Tung YC, Quinlan M, Wisniewski HM, Binder LI. Abnormal phosphorylation of the microtubule-associated protein tau (tau) in Alzheimer cytoskeletal pathology. *Proc Natl Acad Sci U S A*. 1986 Jul;83(13):4913-7. doi: 10.1073/pnas.83.13.4913. PMID: 3088567; PMCID: PMC323854.
- Hahn I, Voelzmann A, Liew YT, Costa-Gomes B, Prokop A. The model of local axon homeostasis - explaining the role and regulation of microtubule bundles in axon maintenance and pathology. *Neural Dev*. 2019 Nov 9;14(1):11. doi: 10.1186/s13064-019-0134-0. PMID: 31706327; PMCID: PMC6842214.
- Harada A, Takei Y, Kanai Y, Tanaka Y, Nonaka S, Hirokawa N. Golgi vesiculation and lysosome dispersion in cells lacking cytoplasmic dynein. *J Cell Biol*. 1998 Apr 6;141(1):51-9. doi: 10.1083/jcb.141.1.51. PMID: 9531547; PMCID: PMC2132725.
- Hausrat TJ, Janiesch PC, Breiden P, Lutz D, Hoffmeister-Ullerich S, Hermans-Borgmeyer I, Failla AV, Kneussel M. Disruption of tubulin-alpha4a polyglutamylation prevents aggregation of hyper-phosphorylated tau and microglia activation in mice. *Nat Commun*. 2022 Jul 20;13(1):4192. doi: 10.1038/s41467-022-31776-5. PMID: 35858909; PMCID: PMC9300677.
- Hernández F, Gómez de Barreda E, Fuster-Matanzo A, Lucas JJ, Avila J. GSK3: a possible link between beta amyloid peptide and tau protein. *Exp Neurol*. 2010 Jun;223(2):322-5. doi: 10.1016/j.expneurol.2009.09.011. Epub 2009 Sep 24. PMID: 19782073.
- Hirano A, et al. Fine structural observations of neurofilamentous changes in amyotrophic lateral sclerosis. *J Neuropathol Exp Neurol*. 1984;43(5):461-470.
- Hirokawa N, Noda Y, Tanaka Y, Niwa S. Kinesin superfamily motor proteins and intracellular transport. *Nat Rev Mol Cell Biol*. 2009 Oct;10(10):682-96. doi: 10.1038/nrm2774. PMID: 19773780.
- Hirokawa N, Niwa S, Tanaka Y. Molecular motors in neurons: transport mechanisms and roles in brain function, development, and disease. *Neuron*. 2010 Nov 18;68(4):610-38. doi: 10.1016/j.neuron.2010.09.039. PMID: 21092854.

- Hu S, Begum AN, Jones MR, Oh MS, Beech WK, Beech BH, Yang F, Chen P, Ubeda OJ, Kim PC, Davies P, Ma Q, Cole GM, Frautschy SA. GSK3 inhibitors show benefits in an Alzheimer's disease (AD) model of neurodegeneration but adverse effects in control animals. *Neurobiol Dis.* 2009 Feb;33(2):193-206. doi: 10.1016/j.nbd.2008.10.007. Epub 2008 Nov 5. PMID: 19038340; PMCID: PMC4313761.
- Huang CF, Banker G. The translocation selectivity of the kinesins that mediate neuronal organelle transport. *Traffic.* 2012 Apr;13(4):549-64. doi: 10.1111/j.1600-0854.2011.01325.x. Epub 2012 Jan 24. PMID: 22212743; PMCID: PMC3967410.
- Huang EJ, Reichardt LF. Trk receptors: roles in neuronal signal transduction. *Annu Rev Biochem.* 2003;72:609-42. doi: 10.1146/annurev.biochem.72.121801.161629. Epub 2003 Mar 27. PMID: 12676795.
- Iqbal K, Grundke-Iqbal I. Alzheimer neurofibrillary degeneration: significance, etiopathogenesis, therapeutics and prevention. *J Cell Mol Med.* 2008 Jan-Feb;12(1):38-55. doi: 10.1111/j.1582-4934.2008.00225.x. Epub 2007 Jan 9. PMID: 18194444; PMCID: PMC3139457.
- Iqbal K, Liu F, Gong CX. Tau and neurodegenerative disease: the story so far. *Nat Rev Neurol.* 2016 Jan;12(1):15-27. doi: 10.1038/nrneurol.2015.225. Epub 2015 Dec 4. PMID: 26635213.
- Jackson GR, Wiedau-Pazos M, Sang TK, Wagle N, Brown CA, Massachi S, Geschwind DH. Human wild-type tau interacts with wingless pathway components and produces neurofibrillary pathology in *Drosophila*. *Neuron.* 2002 May 16;34(4):509-19. doi: 10.1016/s0896-6273(02)00706-7. PMID: 12062036.
- Kalinowska-Lyszczarz A, Losy J. The role of neurotrophins in multiple sclerosis-pathological and clinical implications. *Int J Mol Sci.* 2012 Oct 22;13(10):13713-25. doi: 10.3390/ijms131013713. PMID: 23202976; PMCID: PMC3497350.
- Karpus WJ. Cytokines and Chemokines in the Pathogenesis of Experimental Autoimmune Encephalomyelitis. *J Immunol.* 2020 Jan 15;204(2):316-326. doi: 10.4049/jimmunol.1900914. PMID: 31907274.
- Khan SS, Bloom GS. Tau: The Center of a Signaling Nexus in Alzheimer's Disease. *Front Neurosci.* 2016 Feb 9;10:31. doi: 10.3389/fnins.2016.00031. PMID: 26903798; PMCID: PMC4746348.
- Kim HS, Park CH, Cha SH, Lee JH, Lee S, Kim Y, Rah JC, Jeong SJ, Suh YH. Carboxyl-terminal fragment of Alzheimer's APP destabilizes calcium homeostasis and renders neuronal cells vulnerable to excitotoxicity. *FASEB J.* 2000 Aug;14(11):1508-17. doi: 10.1096/fj.14.11.1508. PMID: 10928985.
- Kreft KL, van Meurs M, Wierenga-Wolf AF, Melief MJ, van Strien ME, Hol EM, Oostra BA, Laman JD, Hintzen RQ. Abundant kif21b is associated with accelerated progression in neurodegenerative diseases. *Acta Neuropathol Commun.* 2014 Oct 3;2:144. doi: 10.1186/s40478-014-0144-4. PMID: 25274010; PMCID: PMC4207309.
- Labonté D, Thies E, Kneussel M. The kinesin KIF21B participates in the cell surface delivery of  $\gamma 2$  subunit-containing GABAA receptors. *Eur J Cell Biol.* 2014 Aug-Sep;93(8-9):338-46. doi: 10.1016/j.ejcb.2014.07.007. Epub 2014 Aug 2. PMID: 25172774.
- Lasagna-Reeves CA, Castillo-Carranza DL, Sengupta U, Sarmiento J, Troncoso J, Jackson GR, Kaye R. Identification of oligomers at early stages of tau aggregation in Alzheimer's disease. *FASEB J.* 2012 May;26(5):1946-59. doi: 10.1096/fj.11-199851. Epub 2012 Jan 17. PMID: 22253473; PMCID: PMC4046102.

- Lauretti E, Dincer O, Praticò D. Glycogen synthase kinase-3 signaling in Alzheimer's disease. *Biochim Biophys Acta Mol Cell Res.* 2020 May;1867(5):118664. doi: 10.1016/j.bbamcr.2020.118664. Epub 2020 Jan 30. PMID: 32006534; PMCID: PMC7047718.
- Lewis J, Dickson DW, Lin WL, Chisholm L, Corral A, Jones G, Yen SH, Sahara N, Skipper L, Yager D, Eckman C, Hardy J, Hutton M, McGowan E. Enhanced neurofibrillary degeneration in transgenic mice expressing mutant tau and APP. *Science.* 2001 Aug 24;293(5534):1487-91. doi: 10.1126/science.1058189. PMID: 11520987.
- Livingston G, Huntley J, Sommerlad A, Ames D, Ballard C, Banerjee S, Brayne C, Burns A, Cohen-Mansfield J, Cooper C, Costafreda SG, Dias A, Fox N, Gitlin LN, Howard R, Kales HC, Kivimäki M, Larson EB, Ogunniyi A, Orgeta V, Ritchie K, Rockwood K, Sampson EL, Samus Q, Schneider LS, Selbæk G, Teri L, Mukadam N. Dementia prevention, intervention, and care: 2020 report of the Lancet Commission. *Lancet.* 2020 Aug 8;396(10248):413-446. doi: 10.1016/S0140-6736(20)30367-6. Epub 2020 Jul 30. Erratum in: *Lancet.* 2023 Sep 30;402(10408):1132. PMID: 32738937; PMCID: PMC7392084.
- Ly PT, Wu Y, Zou H, Wang R, Zhou W, Kinoshita A, Zhang M, Yang Y, Cai F, Woodgett J, Song W. Inhibition of GSK3 $\beta$ -mediated BACE1 expression reduces Alzheimer-associated phenotypes. *J Clin Invest.* 2013 Jan;123(1):224-35. doi: 10.1172/JCI64516. Epub 2012 Dec 3. PMID: 23202730; PMCID: PMC3533290.
- Maday S, Twelvetrees AE, Moughamian AJ, Holzbaur EL. Axonal transport: cargo-specific mechanisms of motility and regulation. *Neuron.* 2014 Oct 22;84(2):292-309. doi: 10.1016/j.neuron.2014.10.019. Epub 2014 Oct 22. PMID: 25374356; PMCID: PMC4269290.
- Mandelkow EM, Mandelkow E. Tau in Alzheimer's disease. *Trends Cell Biol.* 1998 Nov;8(11):425-7. doi: 10.1016/s0962-8924(98)01368-3. PMID: 9854307.
- Marszalek JR, Weiner JA, Farlow SJ, Chun J, Goldstein LS. Novel dendritic kinesin sorting identified by different process targeting of two related kinesins: KIF21A and KIF21B. *J Cell Biol.* 1999 May 3;145(3):469-79. doi: 10.1083/jcb.145.3.469. PMID: 10225949; PMCID: PMC2185086.
- Martin R, Sospedra M, Rosito M, Engelhardt B. Current multiple sclerosis treatments have improved our understanding of MS autoimmune pathogenesis. *Eur J Immunol.* 2016 Sep;46(9):2078-90. doi: 10.1002/eji.201646485. PMID: 27467894.
- Masliah E, Mallory M, Hansen L, Alford M, DeTeresa R, Terry R, Baudier J, Saitoh T. Localization of amyloid precursor protein in GAP43-immunoreactive aberrant sprouting neurites in Alzheimer's disease. *Brain Res.* 1992 Mar 6;574(1-2):312-6. doi: 10.1016/0006-8993(92)90831-s. PMID: 1386275.
- Masucci EM, Relich PK, Lakadamyali M, Ostap EM, Holzbaur ELF. Microtubule dynamics influence the retrograde biased motility of kinesin-4 motor teams in neuronal dendrites. *Mol Biol Cell.* 2022 May 15;33(6):ar52. doi: 10.1091/mbc.E21-10-0480. Epub 2021 Oct 27. PMID: 34705476; PMCID: PMC9265162.
- Meyer-Arndt L, Kerkerling J, Kuehl T, Infante AG, Paul F, Rosiewicz KS, Siffrin V, Alisch M. Inflammatory Cytokines Associated with Multiple Sclerosis Directly Induce Alterations of Neuronal Cytoarchitecture in Human Neurons. *J Neuroimmune Pharmacol.* 2023 Jun;18(1-2):145-159. doi: 10.1007/s11481-023-10059-w. Epub 2023 Mar 2. PMID: 36862362; PMCID: PMC10485132.

- Millecamps S, Julien JP. Axonal transport deficits and neurodegenerative diseases. *Nat Rev Neurosci.* 2013 Mar;14(3):161-76. doi: 10.1038/nrn3380. Epub 2013 Jan 30. PMID: 23361386.
- Mocanu MM, Nissen A, Eckermann K, Khlistunova I, Biernat J, Drexler D, Petrova O, Schönig K, Bujard H, Mandelkow E, Zhou L, Rune G, Mandelkow EM. The potential for beta-structure in the repeat domain of tau protein determines aggregation, synaptic decay, neuronal loss, and coassembly with endogenous Tau in inducible mouse models of tauopathy. *J Neurosci.* 2008 Jan 16;28(3):737-48. doi: 10.1523/JNEUROSCI.2824-07.2008. PMID: 18199773; PMCID: PMC6670355.
- Muhia M, Thies E, Labonté D, Ghiretti AE, Gromova KV, Kompero F, Lappe-Siefke C, Hermans-Borgmeyer I, Kuhl D, Schweizer M, Ohana O, Schwarz JR, Holzbaur ELF, Kneussel M. The Kinesin KIF21B Regulates Microtubule Dynamics and Is Essential for Neuronal Morphology, Synapse Function, and Learning and Memory. *Cell Rep.* 2016 May 3;15(5):968-977. doi: 10.1016/j.celrep.2016.03.086. Epub 2016 Apr 21. PMID: 27117409; PMCID: PMC5305027.
- Neve RL, Selkoe DJ, Kurnit DM, Kosik KS. A cDNA for a human microtubule associated protein 2 epitope in the Alzheimer neurofibrillary tangle. *Brain Res.* 1986 Nov;387(2):193-6. doi: 10.1016/0169-328x(86)90011-2. PMID: 2431745.
- Ni S, Li J, Qiu S, Xie Y, Gong K, Duan Y. KIF21B Expression in Osteosarcoma and Its Regulatory Effect on Osteosarcoma Cell Proliferation and Apoptosis Through the PI3K/AKT Pathway. *Front Oncol.* 2021 Jan 28;10:606765. doi: 10.3389/fonc.2020.606765. PMID: 33585227; PMCID: PMC7879035.
- Nicol B, Salou M, Laplaud DA, Wekerle H. The autoimmune concept of multiple sclerosis. *Presse Med.* 2015 Apr;44(4 Pt 2):e103-12. doi: 10.1016/j.lpm.2015.02.009. Epub 2015 Mar 23. PMID: 25813101.
- Nociti V, Romozzi M. The Role of BDNF in Multiple Sclerosis Neuroinflammation. *Int J Mol Sci.* 2023 May 8;24(9):8447. doi: 10.3390/ijms24098447. PMID: 37176155; PMCID: PMC10178984.
- Okada Y, Yamazaki H, Sekine-Aizawa Y, Hirokawa N. The neuron-specific kinesin superfamily protein KIF1A is a unique monomeric motor for anterograde axonal transport of synaptic vesicle precursors. *Cell.* 1995 Jun 2;81(5):769-80. doi: 10.1016/0092-8674(95)90538-3. PMID: 7539720.
- Phiel CJ, Wilson CA, Lee VM, Klein PS. GSK-3alpha regulates production of Alzheimer's disease amyloid-beta peptides. *Nature.* 2003 May 22;423(6938):435-9. doi: 10.1038/nature01640. PMID: 12761548.
- Regan P, Whitcomb DJ, Cho K. Physiological and Pathophysiological Implications of Synaptic Tau. *Neuroscientist.* 2017 Apr;23(2):137-151. doi: 10.1177/1073858416633439. Epub 2016 Jul 7. PMID: 26908138.
- Robinson AP, Harp CT, Noronha A, Miller SD. The experimental autoimmune encephalomyelitis (EAE) model of MS: utility for understanding disease pathophysiology and treatment. *Handb Clin Neurol.* 2014;122:173-89. doi: 10.1016/B978-0-444-52001-2.00008-X. PMID: 24507518; PMCID: PMC3981554.
- Rosa E, Mahendram S, Ke YD, Ittner LM, Ginsberg SD, Fahnstock M. Tau downregulates BDNF expression in animal and cellular models of Alzheimer's disease. *Neurobiol Aging.* 2016 Dec;48:135-142. doi: 10.1016/j.neurobiolaging.2016.08.020. Epub 2016 Aug 31. PMID: 27676333; PMCID: PMC5159317.

- Saftig P, Klumperman J. Lysosome biogenesis and lysosomal membrane proteins: trafficking meets function. *Nat Rev Mol Cell Biol.* 2009;10(9):623-635. doi:10.1038/nrm2745
- Scheuner D, Eckman C, Jensen M, Song X, Citron M, Suzuki N, Bird TD, Hardy J, Hutton M, Kukull W, Larson E, Levy-Lahad E, Viitanen M, Peskind E, Poorkaj P, Schellenberg G, Tanzi R, Wasco W, Lannfelt L, Selkoe D, Younkin S. Secreted amyloid beta-protein similar to that in the senile plaques of Alzheimer's disease is increased in vivo by the presenilin 1 and 2 and APP mutations linked to familial Alzheimer's disease. *Nat Med.* 1996 Aug;2(8):864-70. doi: 10.1038/nm0896-864. PMID: 8705854.
- Sehar U, Rawat P, Reddy AP, Kopel J, Reddy PH. Amyloid Beta in Aging and Alzheimer's Disease. *Int J Mol Sci.* 2022 Oct 26;23(21):12924. doi: 10.3390/ijms232112924. PMID: 36361714; PMCID: PMC9655207.
- Selkoe DJ. Amyloid protein and Alzheimer's disease. *Sci Am.* 1991 Nov;265(5):68-71, 74-6, 78. doi: 10.1038/scientificamerican1191-68. PMID: 1785042.
- Shima Y, Kawaguchi SY, Kosaka K, Nakayama M, Hoshino M, Nabeshima Y, Hirano T, Uemura T. Opposing roles in neurite growth control by two seven-pass transmembrane cadherins. *Nat Neurosci.* 2007 Aug;10(8):963-9. doi: 10.1038/nn1933. Epub 2007 Jul 8. PMID: 17618280.
- Sorbara CD, Wagner NE, Ladwig A, Nikić I, Merkler D, Kleele T, Marinković P, Naumann R, Godinho L, Bareyre FM, Bishop D, Misgeld T, Kerschensteiner M. Pervasive axonal transport deficits in multiple sclerosis models. *Neuron.* 2014 Dec 17;84(6):1183-90. doi: 10.1016/j.neuron.2014.11.006. Epub 2014 Nov 26. PMID: 25433639.
- Stokin GB, et al. Axonopathy and transport deficits early in the pathogenesis of Alzheimer's disease. *Science.* 2005;307(5713):1282–1288.
- Tejeda GS, Díaz-Guerra M. Integral Characterization of Defective BDNF/TrkB Signalling in Neurological and Psychiatric Disorders Leads the Way to New Therapies. *Int J Mol Sci.* 2017 Jan 28;18(2):268. doi: 10.3390/ijms18020268. PMID: 28134845; PMCID: PMC5343804.
- Tymanskyj SR, Curran BM, Ma L. Selective axonal transport through branch junctions is directed by growth cone signaling and mediated by KIF1/kinesin-3 motors. *Cell Rep.* 2022 Apr 26;39(4):110748. doi: 10.1016/j.celrep.2022.110748. PMID: 35476993; PMCID: PMC9097860.
- Vergara C, Houben S, Suain V, Yilmaz Z, De Decker R, Vanden Dries V, Boom A, Mansour S, Leroy K, Ando K, Brion JP. Amyloid- $\beta$  pathology enhances pathological fibrillary tau seeding induced by Alzheimer PHF in vivo. *Acta Neuropathol.* 2019 Mar;137(3):397-412. doi: 10.1007/s00401-018-1953-5. Epub 2019 Jan 1. PMID: 30599077.
- Wang Y, Mandelkow E. Tau in physiology and pathology. *Nat Rev Neurosci.* 2016 Jan;17(1):5-21. doi: 10.1038/nrn.2015.1. Epub 2015 Dec 3. PMID: 26631930.
- Wloga D, Joachimiak E, Fabczak H. Tubulin Post-Translational Modifications and Microtubule Dynamics. *Int J Mol Sci.* 2017 Oct 21;18(10):2207. doi: 10.3390/ijms18102207. PMID: 29065455; PMCID: PMC5666887.
- Wolfe MS. The role of tau in neurodegenerative diseases and its potential as a therapeutic target. *Scientifica (Cairo).* 2012;2012:796024. doi: 10.6064/2012/796024. Epub 2012 Dec 19. PMID: 24278740; PMCID: PMC3820460.
- Wolk DA, Das SR, Mueller SG, Weiner MW, Yushkevich PA; Alzheimer's Disease Neuroimaging Initiative. Medial temporal lobe subregional morphometry using high resolution MRI in Alzheimer's disease. *Neurobiol Aging.* 2017 Jan;49:204-213. doi:

10.1016/j.neurobiolaging.2016.09.011. Epub 2016 Sep 30. PMID: 27836336; PMCID: PMC5154888.

Yang X, Li M, Wang L, Hu Z, Zhang Y, Yang Q. Association of KIF21B genetic polymorphisms with ankylosing spondylitis in a Chinese Han population of Shandong Province. *Clin Rheumatol.* 2015 Oct;34(10):1729-36. doi: 10.1007/s10067-014-2761-5. Epub 2014 Aug 23. PMID: 25149646.

Zhang K, Foster HE, Rondelet A, Lacey SE, Bahi-Buisson N, Bird AW, Carter AP. Cryo-EM Reveals How Human Cytoplasmic Dynein Is Auto-inhibited and Activated. *Cell.* 2017 Jun 15;169(7):1303-1314.e18. doi: 10.1016/j.cell.2017.05.025. Epub 2017 Jun 8. PMID: 28602352; PMCID: PMC5473941.

## 9. Abstract

The first part investigates KIF21B, a member of the kinesin superfamily of proteins that have been implicated in the pathogenesis of Alzheimer's disease (AD), a progressive neurodegenerative disorder marked by the presence of extracellular amyloid  $\beta$  plaques and intracellular Tau neurofibrillary tangles. The phosphorylation status of Tau, a microtubule-associated protein, is regulated by the Akt/GSK3 $\beta$  signaling pathway. KIF21B has been reported to modulate osteosarcoma cell proliferation and apoptosis through the PI3K/Akt pathway. Therefore, there is a hypothesis that KIF21B may affect PI3K/Akt pathway in hippocampal neurons as well and, as consequence, tau phosphorylation. Western blot analysis and immunohistochemistry performed on KIF21B knockout mice showed reduced levels of phosphorylated Akt (pAkt), raised phosphorylated GSK3 $\beta$  (Tyr216), and increased Tau phosphorylation, thus supporting a signaling pathway linking KIF21B to AD pathogenesis.

The second part explores multiple sclerosis (MS), a common neuroinflammatory disease characterized by progressive axonal degeneration. Extensive transport impairments and reduced supply of distal organelles may contribute to late-stage axonal atrophy in the disease. Genetic variations in the KIF21B gene have been associated with MS and other inflammatory conditions. However, the specific motors affected at the onset of inflammation remain poorly understood. This experiment requires a two-step process to investigate this. The first step was to build a wild-type initial model of neuroinflammation for the experiment, and the second was to base the experiment again on using KIF21B KO cortical neurons. Here, I subjected mouse cortical neurons at the day in vitro (DIV) 12 to chronic (48-hour) application of an inflammatory cocktail (IC) containing IFN- $\gamma$ , TNF- $\alpha$ , IL17 (each at 100nM), or control conditions. I conducted live-cell imaging studies of bidirectional axonal transport of kinesin-dependent synaptophysin, BDNF, N-cadherin, and dynein-dependent LAMP1-driven proteins. Results show no significant differences among them, while velocities of all particles of some cargo display potential differences, necessitating more experiments for result validation.



## 10. Zusammenfassung

Der erste Teil untersucht KIF21B, ein Mitglied der Kinesin-Superfamilie von Proteinen, die in die Pathogenese der Alzheimer-Krankheit (AD) verwickelt sind, einer fortschreitenden neurodegenerativen Erkrankung, die durch das Vorhandensein von extrazellulären Amyloid- $\beta$ -Plaques und intrazellulären neurofibrillären Tau-Tangles gekennzeichnet ist. Der Phosphorylierungsstatus von Tau, einem mit Mikrotubuli assoziierten Protein, wird durch den Akt/GSK3 $\beta$ -Signalweg reguliert. Es wurde berichtet, dass KIF21B die Proliferation und Apoptose von Osteosarkomzellen über den PI3K/Akt-Signalweg moduliert. Daher besteht die Hypothese, dass KIF21B auch den PI3K/Akt-Signalweg in Hippocampus-Neuronen und infolgedessen die Tau-Phosphorylierung beeinflussen könnte. Western-Blot-Analysen und Immunhistochemie, die an KIF21B-Knockout-Mäusen durchgeführt wurden, zeigten reduzierte Werte von phosphoryliertem Akt (pAkt), erhöhte Werte von phosphoryliertem GSK3 $\beta$  (Tyr216) und erhöhte Tau-Phosphorylierung, was einen Signalweg unterstützt, der KIF21B mit der AD-Pathogenese verbindet.

Der zweite Teil befasst sich mit der Multiplen Sklerose (MS), einer häufigen neuroinflammatorischen Erkrankung, die durch eine fortschreitende axonale Degeneration gekennzeichnet ist. Weitreichende Transportstörungen und eine verminderte Versorgung mit distalen Organellen können zur axonalen Atrophie im Spätstadium der Krankheit beitragen. Genetische Variationen im KIF21B-Gen wurden mit MS und anderen Entzündungskrankheiten in Verbindung gebracht. Die spezifischen Motoren, die beim Ausbruch der Entzündung betroffen sind, sind jedoch noch nicht ausreichend bekannt. Dieses Experiment erfordert einen zweistufigen Prozess, um dies zu untersuchen. Der erste Schritt bestand darin, ein Wildtyp-Ausgangsmodell der Neuroinflammation für das Experiment zu erstellen, und der zweite bestand darin, das Experiment wiederum auf die Verwendung von KIF21B KO-Kortikalneuronen zu stützen. Hier habe ich kortikale Neuronen der Maus am 12. Tag *in vitro* (DIV) einer chronischen (48-stündigen) Anwendung eines Entzündungscocktails (IC) mit IFN- $\gamma$ , TNF- $\alpha$ , IL17 (jeweils 100nM) oder Kontrollbedingungen unterzogen. Ich führte Live-Cell-Imaging-Studien zum bidirektionalen axonalen Transport von Kinesin-abhängigem Synaptophysin, BDNF, N-Cadherin und Dynein-abhängigen LAMP1-getriebenen Proteinen durch. Die Ergebnisse zeigen keine signifikanten Unterschiede zwischen ihnen, während die

Geschwindigkeiten aller Partikel einiger Ladungen potenzielle Unterschiede aufweisen, was weitere Experimente zur Validierung der Ergebnisse erforderlich macht.

## 11. Acknowledgements

Studying abroad for my MD has represented a profound and enriching journey, fostering personal growth and providing invaluable insights into my future trajectory. I am grateful for the support and trust from Prof. Matthias Kneuseel to let me take part in this scientific venture. The advancement of my professionalism will now be facilitated to continue further with unshaken patience, which was most needed in the encountered hurdles on my professional way. I am equally grateful for Dr. Kira Gromova Brune, whose expertise proved instrumental in shaping the trajectory of my MD project.

I'm also letting you know that I'm acknowledging Professor Dr. Meliha Karsak, whose initial offer paved the way for my academic pursuits. Furthermore, I sincerely thank the China Scholarship Council (CSC) for its financial support, without which the successful completion of my MD in Germany would not have been feasible.

Gratitude extends to my colleagues in the laboratory, particularly to Deniele, whose mentorship encompassed teaching invaluable lab techniques and promoting a supportive friendship. I especially appreciate Yipeng's invaluable assistance in navigating the laboratory environment. I would also like to thank Yvonne and Christoph for the technical expertise and patience they demonstrated in imparting essential laboratory techniques. Thanks to Dominik and Oliver for their companionship and collaborative spirit and for going beyond laboratory confines to enrich daily life experiences. Gratitude is also extended to Noelia, Alina, and Rebecca for their friendship and companionship post-work hours.

Lastly, I express profound appreciation to my family for their unwavering encouragement and firm support, enabling steadfast focus and dedication to academic pursuits during the challenges of studying abroad. Their encouragement has been a great motivation throughout my educational journey.

## **12. Curriculum Vitae**

### **Personal Information**

Name: Yao Chen

Date of Birth: 21.10.1992

Gender: Female

Nationality: Chinese

Email: yao.chen@zmnh.uni-hamburg.de; yaochen9210@gmail.com

Telephone: +49 01628993406; +86 18702071021

### **Educational Background**

2021-2024: MD study at University Medical Center Hamburg-Eppendorf, Hamburg, Germany

2016-2019: Master of Clinical Medicine (Anesthesiology), Sun Yat-sen University, Guangzhou, PR of China

2010-2016: Bachelor of Clinical Medicine, University of South China, Hengyang, PR of China

### **Research Experience**

2022-2024: The potential role of kinesin family member 21B in neurodegenerative disease, Center for Molecular Neurobiology Hamburg (ZMNH), Institute for Molecular Neurogenetics, Prof. Dr. Matthias Kneussel

2021-2022: The molecular mechanism and therapeutic potential of the cannabinoid receptor CB2 in glioblastoma cells, Center for Molecular Neurobiology Hamburg (ZMNH), Group of Neuronal and Cellular Signal Transduction, Prof. Dr. Meliha Karsak.

2016-2017: Biomolecular cell experiments in the Institute of Neuroscience, School of Medicine, Sun Yat-sen University, Prof. Dr. Jianqiang Feng.

2013-2015: A study on the antagonistic efficacy of H<sub>2</sub>S on restraint stress-induced depression and cognitive impairment in mice by observing the degree of depression of mice in behavioral experiment, Institute of Cognition and Nervous system diseases, School of Medicine, University of South China, Prof. Dr. Xiaoqing Tang.

### **13. Eidesstattliche Erklärung**

Ich versichere ausdrücklich, dass ich die Arbeit selbständig und ohne fremde Hilfe verfasst, andere als die von mir angegebenen Quellen und Hilfsmittel nicht benutzt und die aus den benutzten Werken wörtlich oder inhaltlich entnommenen Stellen einzeln nach Ausgabe (Auflage und Jahr des Erscheinens), Band und Seite des benutzten Werkes kenntlich gemacht habe.

Ferner versichere ich, dass ich die Dissertation bisher nicht einem Fachvertreter an einer anderen Hochschule zur Überprüfung vorgelegt oder mich anderweitig um Zulassung zur Promotion beworben habe.

Ich erkläre mich einverstanden, dass meine Dissertation vom Dekanat der Medizinischen Fakultät mit einer gängigen Software zur Erkennung von Plagiaten überprüft werden kann.

*Yao Chen*

Unterschrift: .....